Final Progress Report

Tailored Bioblendstocks with Low Environmental Impact to Optimize MCCI Engines

Federal Agency	US Department of Energy, Bioenergy Technology Office
Recipient Organization Street Address City and County State and Zip + 4	Regents of the University of Michigan 3003 S. State St. Ann Arbor, MI 48109-1274
FOA Number: Award Number:	DE-FOA-0001919 DE-EE0008482
Project Title:	Tailored Bioblendstocks with Low Environmental Impact to Optimize MCCI Engines
Business Officer and contact information:	Kellie Buss, CRA Regents of the University of Michigan
Project Director/Principal Investigator	André L. Boehman Department of Mechanical Engineering University of Michigan
DUNS:	073133571
Project Start / End Date	10/1/2018 - 6/30/2023
Reporting Period, End Date	Final: June 30th, 2023

Submitted by: André L. Boehman (PI)

Acknowledgement

This material is based upon work supported by the U.S. Department of Energy's Office of Energy Efficiency and Renewable Energy (EERE) under the Fiscal Year 2018 Advanced Vehicle Technologies Research Funding Opportunity Announcement (FOA) Number: DE-FOA-0001919, Area of Interest 5b: Bioblendstocks to Optimize Mixing Controlled Compression Ignition (MCCI) Engines, under Award Number DE-EE0008482.

EXECUTIVE SUMMARY

Objectives

The overall objective of the project is to develop and demonstrate a microalgae bio-blendstock with greater than 60% greenhouse gas reduction potential relative to petroleum diesel, that can reduce sooting propensity, increase cetane number and improve engine thermal efficiency relative to a baseline diesel engine operating on conventional fuel.

Additional objectives include:

- Develop a new framework for both LCA and TEA that explicitly considers temporal variation in productivity and the frequency of crop loss, building upon existing models already developed by the DOE and Argonne National Laboratory
- Determine how fuel compounds that can be produced from the algal biomass can be 'bio-tailored' based on the species composition and biological production process, as well as subsequent processing via HTL to biocrude, and upgrading of the biocrude
- Execute a feedback loop (algae production → biocrude refining → combustion optimization → feedback to refining stage), for optimization of fuels to support mixing-controlled compression-ignition (MCCI) combustion processes
- Optimize MCCI combustion and emissions performance, accounting first for the biological processes that dictate the chemical composition of biocrude oil, and second for the subsequent chemical processes that comprise mixing-controlled compression ignition combustion, including atomization, soot formation, in-cylinder heat transfer, and autoignition characteristics, and the dependence of these processes on the physical and chemical properties of fuels
- Characterize the impact of the model and optimized algal fuels on the sooting tendency of a base fuel, to understand how the molecular structure of these fuels influences soot formation
- Simulate the CFR engine with a simulation tool that permits the validation of reduced kinetic mechanism that capture the full range of low, intermediate and high temperature oxidation
- Simulate MCCI engine combustion processes to demonstrate the incorporation of relevant fuel chemistry that captures the specific impacts of a set of the model and optimized algal fuels, while improving computational speed and predictive capability

Outcomes

Overall, the project achieved the proposed objectives including producing the final tangible deliverable. A sample of algal bioblendstock was analyzed by National Renewable Energy Laboratory (NREL) staff and partners at Yale University. In addition, the work outlined in this report provides substantial new knowledge on the subjects of algae cultivation, algae conversion to biocrude, biocrude upgrading and combustion optimization.

- SOPO Task 1: Demonstration Project

  Consistent with the premise of using a multispecies consortium ("polyculture") of algae to improve robustness during algae cultivation, this project has shown that biological engineering of a multispecies consortium of algae has a greater positive impact on LCA metrics than chemical control of the fungal pathogen using a fungicide.

- SOPO Task 2: Hydrothermal Liquefaction of Wet Algae to Biocrude

  Multispecies consortium algae-targeted hydrothermal liquefaction (HTL) recipes were optimized regarding the biocrude yield rate and quality, and the optimized recipe was verified using the scale-up reactor.

- SOPO Task 3: Life-cycle Assessment and Techno-Economic Analysis

  Consistent with the premise of using a multispecies consortium ("polyculture") of algae to improve robustness during algae cultivation, this project has shown that ecological engineering of a multispecies consortium of algae has a greater positive impact on LCA metrics than chemical control of the fungal pathogen using a fungicide. The LCA greenhouse gas footprint and TEA minimum fuel selling price (MFSP) for fuel production at this bench scale are not near the targets for these measures. However, outcomes from scale-up studies indicate that the LCA GHG footprint will be maintained better with ecological engineering than with chemical control when disease is accounted for during cultivation, and that the projected MFSP will be within the target range when prodiction is at scale.

- SOPO Task 4: Biocrude Upgrading to Tailored Fuels

  The catalyst screening tests were conducted for the best hydrodeoxygenation (HDO) and hydrodesulfurization (HDS) efficiency, and the best-fit catalyst (Ni/SiO_2-Al_2O_3) for the multispecies consortium algae was selected among 10 catalyst candidates. The optimized catalytic upgrading recipe was verified to be the best result in the scale-up reactor experiments, and the upgraded fuels were successfully distilled for ready-to-use diesel fuel.

  Analyses of the sample of upgraded, distilled, algal bioblendstock for MCCI combustion were performed by staff at the National Renewable Energy Laboratory. We were not able to meet the 500 ml target of bioblendstock, but around 130 ml of sample was produced (100 ml from an algal polyculture and 30 ml from an algae monoculture), which is an adequate amount for the property analyses given the techniques used at NREL.

- SOPO Task 5: Engine Studies and Simulation

  Using both a light-duty multi-cylinder turbodiesel engine and a single-cylinder heavy-duty diesel engine, improvements in thermal efficiency and reductions in soot emissions (while maintaining NOx parity) have been demonstrated using a 30 vol.% blend of a model of our algal bioblendstock and using a new renewable diesel fuel (which represents a model for application of 100% optimized renewable fuel). In the heavy-duty test engine, reductions in fuel consumption were observed by as much as 6% with the 30 vol.% model algal bioblendstock and as much as 8% with 100% renewable diesel fuel.

TABLE OF CONTENTS

1. ACCOMPLISHMENTS

At the conclusion of the project, the final milestone related to the production of the optimized algal bioblendstock and transfer of a sample to the DOE National Lab Team (led by Dr. R. McCormick, NREL) was completed. The sample was be sent to NREL for analyses. Also at the conclusion of the project, we reported at a technical conference the completion of a directly related milestone of demonstration of optimized MCCI combustion with a model for the algal bioblendstock. A listing of these final project milestones is included in Appendix A.

With the completion of these milestones, all of the milestones outlined in the SOPO have been completed.

This work has been published and presented in a number of forums. The References Cited (Section 4 of this report) lists some of the publications.

- Dow Sustainability Program Distinguished Scholars and Faculty Dinner, "Toward sustainable transportation". February 20, 2019.

- Chalmers University of Technology, Combustion Engine Research Center Annual Seminar, "Autoignition Characteristics of Alternative Fuels". May 28, 2019.

An abstract was submitted for the American Chemical Society National Meeting for a symposium on *Chemistry of Fuel Properties, Combustion & Fuel-Engine Interactions*, that was to be held March 22-26, 2020, in Philadelphia, PA. That symposium was organized by André Boehman, Dan Gaspar, Seonah Kim and Bob McCormick (Gaspar and McCormick being DOE leaders of the Co-Optima program). Our team's abstract was titled:

- "Tailored Bioblendstocks with Low Environmental Impact to Optimize MCCI Engines"

We gave a technical presentation on July 28, 2020 in a Co-Optima teleconference that took the place of the March 2020 All Hands Meeting that had to be transitioned to a virtual meeting.

We gave a technical presentation on March 16, 2021, in the DOE BETO Bi-Annual Review Meeting in the Co-Optima session.

In April 2021, again a symposium was held on *Chemistry of Fuel Properties, Combustion & Fuel-Engine Interactions* in conjunction with the Energy & Fuels Division of the ACS. We presented on our project again, with updated content to present progress since the previous symposium in 2020.

We presented our project progress again on September 28, 2021 for a Co-Optima Stakeholders meeting.

Discussion of this project has been included in invited talks at multiple conferences in Fall 2022, including a department seminar at Marquette University and a plenary talk at the EXPOIngeneria in Medellin, Colombia. Both talks were on the subject of "Reducing GHG Emissions via Low Carbon Fuels: Challenges and Opportunities." Another talk that included some outcomes from this project was presented at the 4th International Biofuels Conference in, In Cali, Colombia in April 2023.

Finally, an additional talk based on this work will be given at the ACS National Meeting in San Francisco in a Co-Optima themed session in August 2023.

The following is a consolidated listing of products (technical papers and conference presentations and posters generated that directly come from the work performed in this study.

Refereed Technical Papers

Widin, S.L., Billings, K.M., McGowen, J., Cardinale, B.J. Biodiversity and disease risk in an algal biofuel system: An experimental test in outdoor ponds using a before-after-control-impact (BACI) design. PLoS ONE 17(4): e0267674 (2022). https://doi.org/10.1371/journal.pone.0267674

Miyasato E. M., Cardinale, B. J. Impacts of Fungal Disease on Algal Biofuel Systems: Using Life Cycle Assessment to Compare Control Strategies, *Environmental Science & Technology 57*(6), 2602-2610 (2023). DOI: 10.1021/acs.est.2c07031

Thomas, P. K., D. C. Hietala, and B. J. Cardinale. Tolerance to allelopathic inhibition by free fatty acid in five biofuel candidate microalgae strains. *Bioresource Technology Reports*, 21:101321) 2023). (http://dx.doi.org/10.2139/ssrn.4269951).

Doctoral Theses Completed

Han, J. CFD Modeling of Ignition and Soot Formation for Advanced Compression-Ignition Engines. Ph.D. Thesis, Mechanical Engineering, Penn State University (2022).

Masters Theses Completed

Miyasato, E. Impacts of fungal disease on algal biofuel systems: Using life-cycle assessment to compare control strategies. *University of Michigan, School for Environment and Sustainability,* Ann Arbor, Michigan (2023).

Widin, S. L. Biodiversity and disease risk in an algal biofuel system: An experimental test in outdoor ponds using a before-after-control-impact (BACI) design. *University of Michigan, School for Environment and Sustainability,* Ann Arbor, Michigan (2022).

Conference Posters and Presentations

Boehman, A.L., Haworth, D.C., Savage, P., Cardinale, B., Thompson, L. “Tailored Bioblendstocks with Low Environmental Impact to Optimize MCCI Engines,” DOE Co-Optima All-Hands Meeting (virtual), July 28, 2020.

Boehman, A.L., Haworth, D.C., Savage, P., Cardinale, B., Thompson, L. “Tailored Bioblendstocks with Low Environmental Impact to Optimize MCCI Engines,” DOE BETO Bi-Annual Review Meeting, Denver, CO, March 16, 2021.

Boehman, A.L., Haworth, D.C., Savage, P., Cardinale, B., Thompson, L. “Tailored Bioblendstocks with Low Environmental Impact to Optimize MCCI Engines,” DOE Co-Optima All-Hands Meeting, Oak Ridge, TN, September 28, 2021.

Abdullah, M., Boehman, A.L. “Utilizing data-based modeling with low life cycle GHG emissions algae biofuels for engine optimization”, ACS National Meeting, San Francisco, CA, August 16, 2023.

2. REVIEW OF RESEARCH ACTIVITIES BY SOPO TASK

This section provides a summary of major activities and major findings, challenges and outcomes from each task in the project, covering: Task 1: the ecological engineering of algae cultivation; Task 2: hydrothermal liquefaction for conversion of algae to biocrude; Task 3: life cycle and technoeconomic analysis of cultivation; Task 4: algae upgrading to fuel; and Task 5: experimental and numerical investigations of MCCI combustion.

Task 1. Demonstration Project

Year 1's effort on the demonstration project started on June 7th, 2019, at the Arizona Center for Algae Technology and Innovation (AzCATI). The project was set up according to a BACI experimental design (Before, After, Control, Impact) with three 4.2-m^2 ponds established as algal monocultures of *Selenastrum capricornutum* (Control), and three additional 4.2-m^2 ponds established as algal polycultures with equal inoculums of *Selenastrum capricornutum*, *Scenedesmus obliquus*, and *Chlorella sorokiniana* (Impact). Ponds were monitored for 21 days with weekly harvests of feedstock Before and After they were intentionally infected with an aphelid fungus on July 5th to determine their susceptibility to disease

The demonstration project ended on July 26th, 2019 and was highly successful. Biological and chemical samples from the project were processed from September 2019 through March, 2020. The COVID-19 pandemic slowed the final processing of samples due to shut down of research labs at the University of Michigan. However, two graduate students working on the project set-up make-shift microscopy labs in their homes and completed the counts of algal densities and estimates of fungal infection.

Data analyses for the demonstration project were completed, and reported in a paper by Widin et al. [1]. That paper shows that two of three species of algae used in the experiment (*Scenedesmus obliquus* and C*hlorella sorokiniana*) were highly susceptible to fungal disease, whereas a third species (*Selenastrum capricornutum*) was highly resistant to disease. Algal polycultures containing the disease resistant alga *S. capricornutum* were able to persist despite infection, and sustainably produced the target levels of feedstock at productivities of 12 g m^{-2} day^{-1}, as shown in Figure 1. By the end of the experiment, the algal polyculture was mostly composed of *Selenastrum capricornutum,* as the other more susceptible species were wiped-out by disease. The project produced a total 51.6 kg of algal feedstock (29.45 kg from the monoculture, 22.15 kg from the polyculture) as documented in Table 1, which was sufficient for use in subsequent tasks.

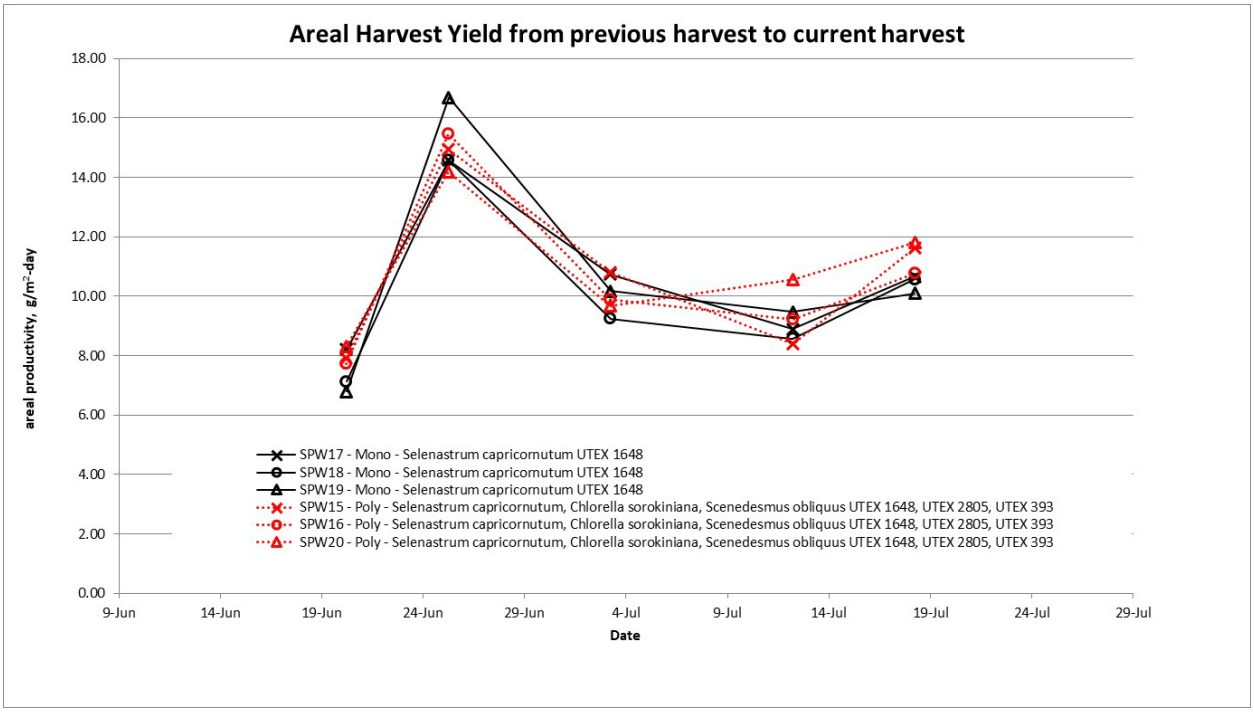

Figure 1. Harvest results from the Demonstration Project showing that we met/exceeded the areal productivity at one harvest during the cultivation study.

Table. Mass of feedstock (kg) harvested from racewa ponds during 2019 DOE experiment at AzCATI. These are the feedstock that was sent to Saemin at U of M f processing via HTL.

Date	Mono	Poly	Total
6/20/2019	5.5	3.0	8.5
6/25/2019	3.0	2.0	5.0
7/3/2019	5.5	4.0	9.5
7/12/2019	6.3	4.5	10.8
7/18/2019	4.6	4.8	9.4
7/25/2019	4.6	3.9	8.5
Average per harvest	4.9	3.7	8.6
Sum of all harvests	34.4	25.8	60.2

Table 1. Harvest yields, showing that we met the yield target during most of the harvests.

Their pond

Our pond

Figure 2. Photographs demonstrating the unique success of the project team during the Demonstration Project at AzCATI in 2019. Only our team's ponds remained healthy throughout the cultivation study.

Our research activities resumed at Arizona State University's Arizona Center for Algae Technology (AzCATI) facility in summer 2021. Our objective in the return to AzCATI was to perform a follow-up demonstration project in commercial-scale raceway ponds with the goal of confirming or modifying our 2019 results that showed multi-species consortia do not confer an advantage over monocultures that are managed with fertilizers and pesticides. This study was performed in small ponds (e.g., 1,200-L, 4.2 m^2) with saline-tolerant algae species. As in the initial demonstration project activity, this follow-up effort was designed as a BACI study (Before, After, Control, Impact) to allow for rigorous statistical inference, so that we can compare performance of the single best species monoculture and best polyculture we have developed with respect to productivity, stability, HTL biocrude quality, and nutrient recycling. Figure 3 shows a photo of students from our team at AzCATI with one of the ponds in operation.

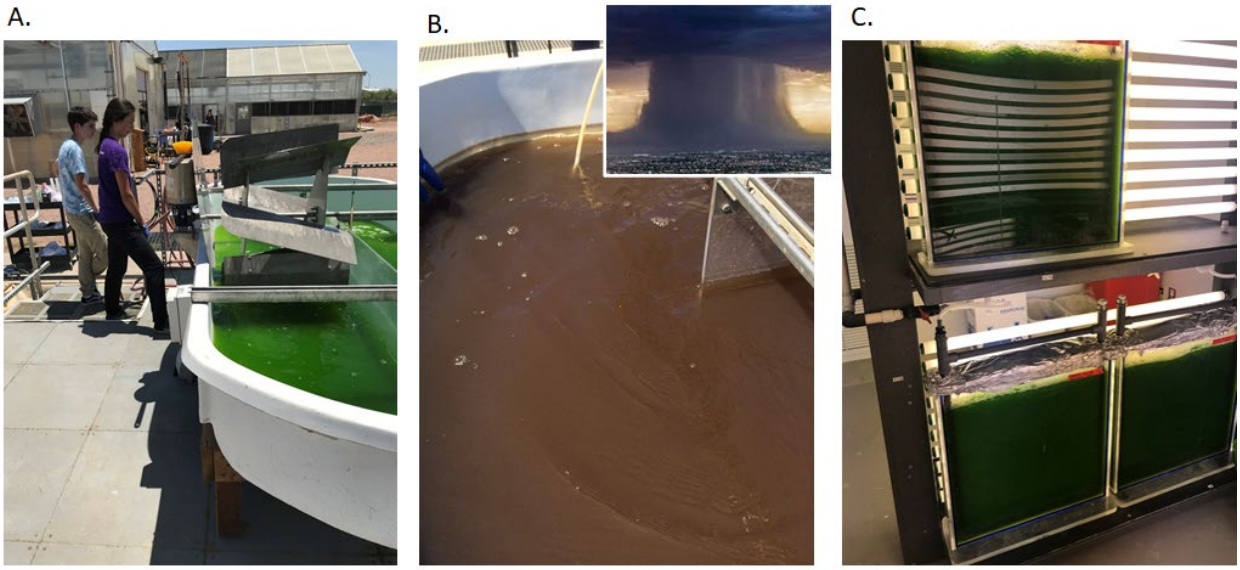

Figure 3. In 2021, we set up 3 experiments in open raceway ponds at the Arizona Center for Algae Technology Innovation (AzCATI) designed to test how mixed-species cultures of estuarine algae stability feedstock production against fungal disease (panel A). Unfortunately, an active summer monsoon season in Arizona decimated feedstocks in outdoor open ponds (panel B). Even so, we were successful in completing several indoor, laboratory based experiments in photobioreactors that challenged mono- and mixed sepcies feedstocks with known strains of chydrid and asselid fungi. These experiments have provided mechanistic insights that have helped to interpret our 2019 campaign at AzCATI in which we were successful at completing outdoor pond experiments using several species of freshwater algae.

The outcomes from Summer 2021 were not as good as in Summer 2019 due to monsoon rains that brought sediment and microorganisms into the ponds at AzCATI. A summary of the outcomes and from Summer 2021 are as follows:

1. In 2021, we repeated our 2019 experiments in which we pitted the most productive algal monocultures against the most productive mixed species cultures in 4.2 m2, 1,200-L outdoor raceway ponds (Figure 1A). Our goal was to determine whether the mixed species cultures would not only be more productive, but more stable through time (i.e. resistant to a crash) when intentionally infected with fungi that routinely lead to crop failure.

2. The main difference between our 2019 and 2021 experiments is that in 2019 we used freshwater algal species, whereas this year we focused on comparable species (*Scenedesmus obliquus*, *Selenastrum capricornutum*, and *Chlorella vulgaris*), but used strains that are adapted for estuarine environments.

3. Unfortunately, Arizona experienced an abnormally active monsoon season that made it difficult to complete experiments. We set up a total of 3 experiments, but each time unpredicted storm events deposited large amounts of sand and debris into the ponds (Figure 1B). With that came

unwanted contamination by multiple types of bacteria, fungi, amoeba, and ciliates that tended to infect or eat the feedstocks. We were not able to maintain feedstocks long enough to complete a BACI designed experiment as planned. We looked at data from these open pond experiments to determine if anything can be stated about the difference between mono- vs. mixed species cultures in their ability to resist contamination imposed on the ponds by natural storm events.

4. While the outdoor, raceway pond experiments did not go as planned, we were successful in completing several indoor, laboratory based experiments in photobioreactors that challenged mono- and mixed species feedstocks with known strains of chydrid and asselid fungi (Figure 3c). These experiments provided important mechanistic insights that help us interpret our 2019 campaign at AzCATI in which we were successful at completing outdoor pond experiments using several species of freshwater algae. A key conclusion is that our analyses show that biological engineering of a multispecies consortium of algae has a greater positive impact on LCA metrics than chemical control of the fungal pathogen using a fungicide [2].

Task 2. Hydrothermal Liquefaction of Wet Algae to Biocrude

In the first year, we identified the species from HTL processing of monoculture and polyculture algae reaction (350 °C for 30 min, small size reactor) using GC-MS. The results are summarized in Figures 4 and 5 and Tables 2 and 3. For both the monoculture and the polyculture samples, one of the most abundant compounds is n-hexadecanoic acid. This is likely a derivative of triglyceride lipids stored in most biological species. Other compounds include long carbon chain compounds with various terminal groups such as carboxylic acids, amides, and alcohols. These are all compounds that arise through substitution and hydrolysis reactions that occur during HTL. This data was compared to the scale-up reactor experiments and the most abundant compounds were well matched.

Table 2. Monoculture *S. capriconutum* GCMS Results				
Peak #	R. Time	% Area	Likely Compound	Similarity Index
3	20.232	3.99	1-Pentadecene	96
9	26.354	1.89	3,7,11,15-tetramethyl-hexadecyl acetic acid	89
11	26.543	4.48	R,R,R,R-3,7,11,15-E-2-tetramethylhexadecene	93
12	26.778	3.81		92
15	**29.008**	**23.03**	**n-hexadecanoic acid**	**97**
16	**31.756**	**21.84**	**Oleic acid**	**90**
17	32.025	3.42	Octadecanoic acid	90
18	32.177	3.19	Hexadecanamide	95
19	32.645	1.90	N-methyl-myristamide	92
23	35.186	2.66	N-butyl-dodecanamide	81
29	39.449	1.47	3-amino-3-(4-octyloxy-phenyl)-propionic acid	75
30	39.983	1.41	Tetracosanoic acid	66
32	41.002	2.31	O-methyl-delta,tocopherol	83
34	42.604	2.18	Octadecanamide	73
38	44.704	1.51	4-pentenoic acid, 2,2-diethyl-3-oxo-5	79

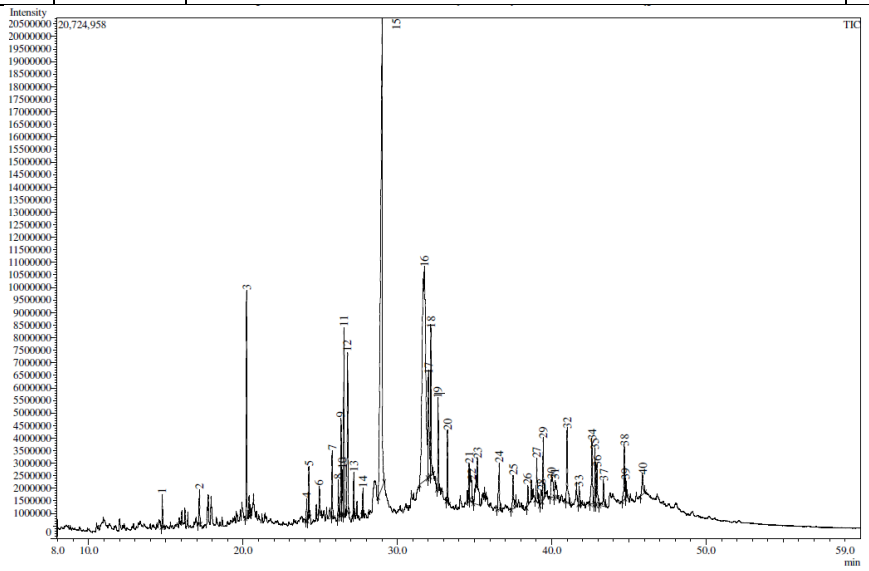

Figure 4. Total Ion Chromatogram of HTL biocrude from monoculture *S. capriconutum,* ran 10/28/19

Table 3. Polyculture *S. capriconutum, C. sorokiniana, S. obliquus* GCMS Results				
Peak #	R. Time	% Area	Likely Compound	Similarity Index
8	17.905	1.84	3-methyl-indole	96
11	20.232	1.94	1-pentadecene	96
14	26.784	1.74	R,R,R,R-3,7,11,15-E-2-tetramethylhexadecene	86
17	**29.138**	**23.00**	**n-hexadecanoic acid**	**95**
19	**31.829**	**23.11**	**Oleic acid**	**89**
20	32.120	2.05	Octadecanoic acid	90
21	32.266	7.36	Hexadecanamide	95
22	32.520	1.36	3,9-dodecadiyne	61
23	32.704	3.90	N-methyl-myristamide	92
24	32.934	2.09	(Z,Z)-9,12-octadecadienoic	75
25	33.300	2.66	N,N-dimethyldodecanamide	90
27	34.573	1.35	N-propylmyristamide	75
28	34.697	1.44	(Z)-9-octadecenamide	83
29	34.853	1.74	9,12,15-octadecatrienoic acid	84
30	35.224	3.30	N-butyl-dodecanamide	82

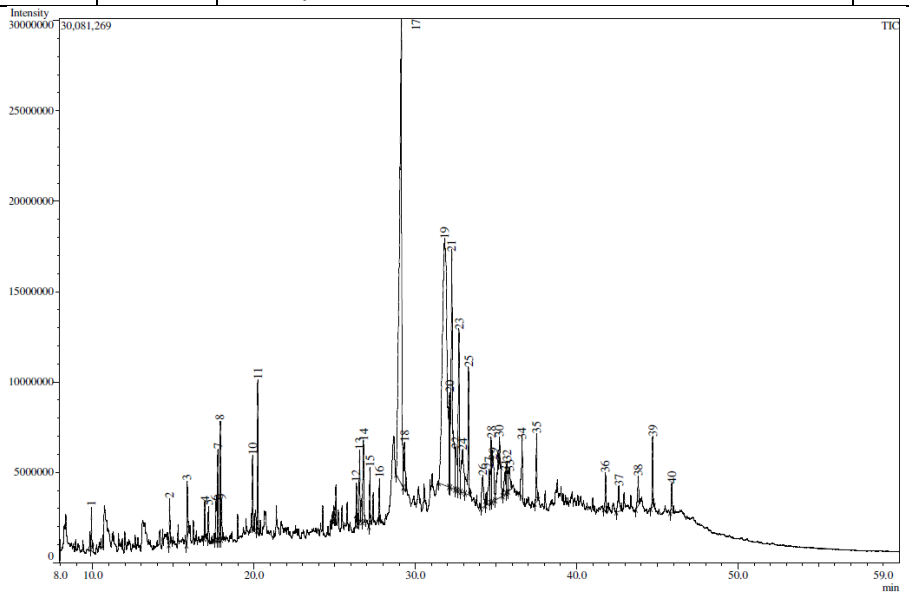

Figure 5. Total Ion Chromatogram of HTL biocrude from polyculture *S. capriconutum, C. sorokiniana, S. obliquus,* ran 10/28/19

Using the small-scale batch reactor, we used our most advanced model for hydrothermal liquefaction to identify reaction conditions that maximized the recovery of chemical energy in the biocrude oil from HTL in the reactor at the University of Michigan. This analysis included the heating profile experienced by that reactor. We determined optimal HTL conditions for a set of different feedstocks to assess the influence of the biochemical composition of the microalgae on these optimal conditions. Table 4 gives the results. The runs directly relevant to this project

are the first two rows in Table 4, which give results for a monoculture of *Selenastrum capricornutum* and a polyculture of *Selenastrum capricornutum*, *Scenedesmus obliquus*, and *Chlorella sorokiniana*. The biochemical composition used in the model for the monoculture and polycultures are estimates based on literature data, and we are analyzing the polyculture to determine the exact composition. Other example data from literature is used to demonstrate possible time and temperature conditions for HTL of algal biomass.

Table 4: The optimized time and temperature for microalgal biomass feedstocks

Feedstock	Pro wt%	Lip wt%	Carb wt%	Time (min)	Final Temp (°C)
Monoculture	27	11	51	83.9	281.6
Polyculture	43	14	31	60.0	282.4
Defatted Chlorella	63	4	35	180.0	252.2
Chlorella Vulgaris	55	25	9	120.0	258.9
Scenedesmus	11	41	36	180.0	268.0

Transition to Scale-Up Reactors

Through the collaboration with the microscale reactor results, we developed the optimized scale-up reactor HTL recipes and protocols for the best yield rate and post HTL biocrude quality. Based on the maximum loading rate (900mL) protocol, we have been boosting biocrude production through HTL. The established protocol for the large-scale HTL is summarized below, and the time-based Pressure-Temperature (P-T) trajectory is shown in Figure 6, which illustrates the P-T curve of the 900mL protocol on the phase diagram of water. The pressure and temperature condition of the HTL process is following a borderline between the liquid and gas phase of the water on the liquid side, and the required time for reaching the 320dC target temperature is 70 minutes, and the total time is 100 mins up to 350dC. The biocrude yield amount per reaction is between 15g and 20g from 900mL of the wet algae, and we have produced more than 250g of the biocrude up to the present.

The protocol for the large-scale HTL runs:

- Final temperature: 350°C (320°C + 30 mins)
- Hold time at 350 °C: None
- Cool down time from 350°C to 130°C: 150 mins
- Final Pressure: 2350 ~ 2400 psig (= 162 ~ 165 bar)
- Wet algae loading: 900 ml
- Stirring speed: 200 rpm

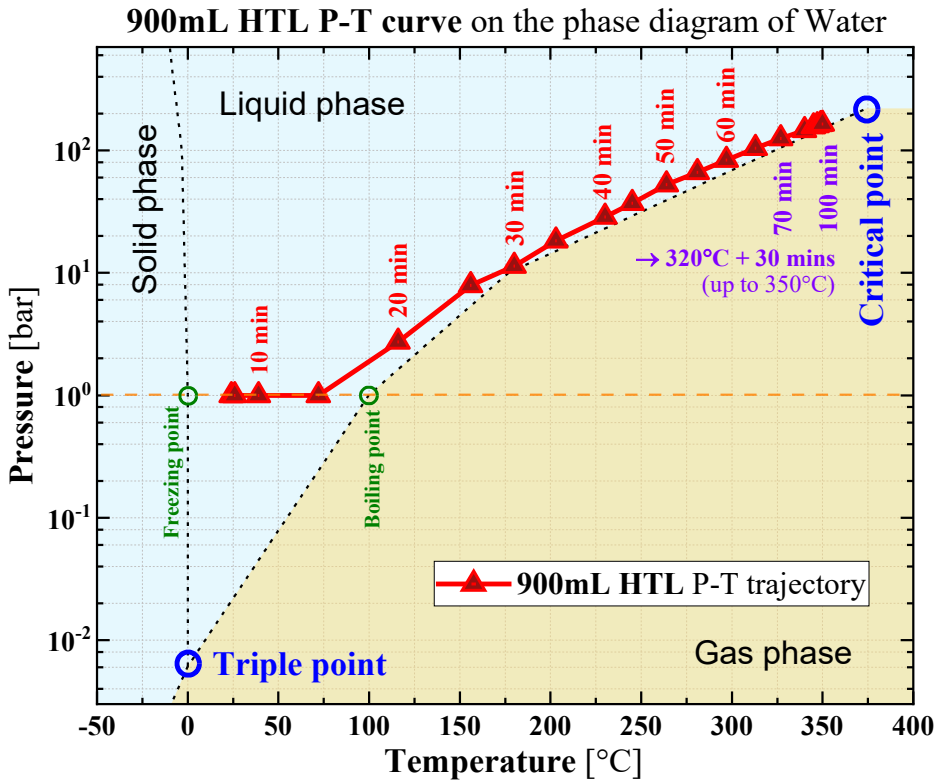

Figure 6. Pressure and temperature trajectory of the 900 mL HTL on the phase diagram of water (H_2O).

The optimized protocols for the filtration and biocrude collection are summarized below. Figure 7 shows the wet algae HTL result (a) and the upgraded separation process using a separatory funnel (b). Before applying the separatory funnel, extracting the biocrude in DCM (dichloromethane) was not smooth because the top layer of the biocrude was not easy to sort out from the sludge layer using a pipette, so there was a bit of biocrude loss in the filtration process. After using the separatory funnel, the separation quality between the two layers is significantly improved. The second filtering process optimization is collecting the solidified biocrude from the filtration process. Figure 8 (a) depicts the filtered sediment on the 2.5µm filter paper. Previously we disposed of the filtered products, but we added one more procedure that dissolved the solidified biocrude around the sludge using additional DCM. After optimizing the filtration process, the biocrude (shown in Figure 8 (b)) yield rate was improved by approximately 30%.

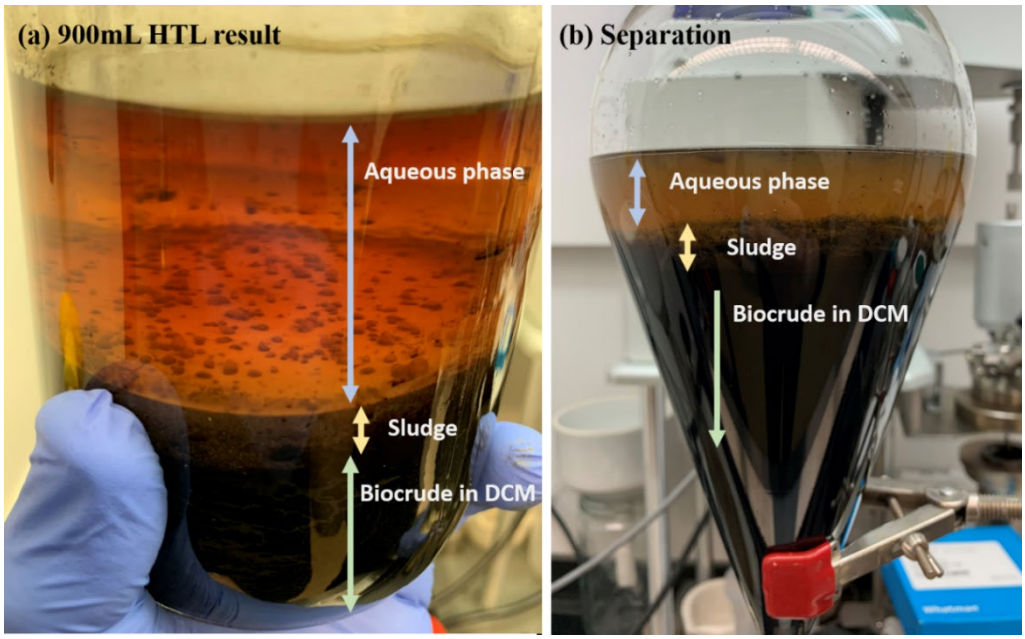

Figure 7. Phase separation of the HTL result: (a) after DCM addition, (b) upgraded filtration process using a separatory funnel.

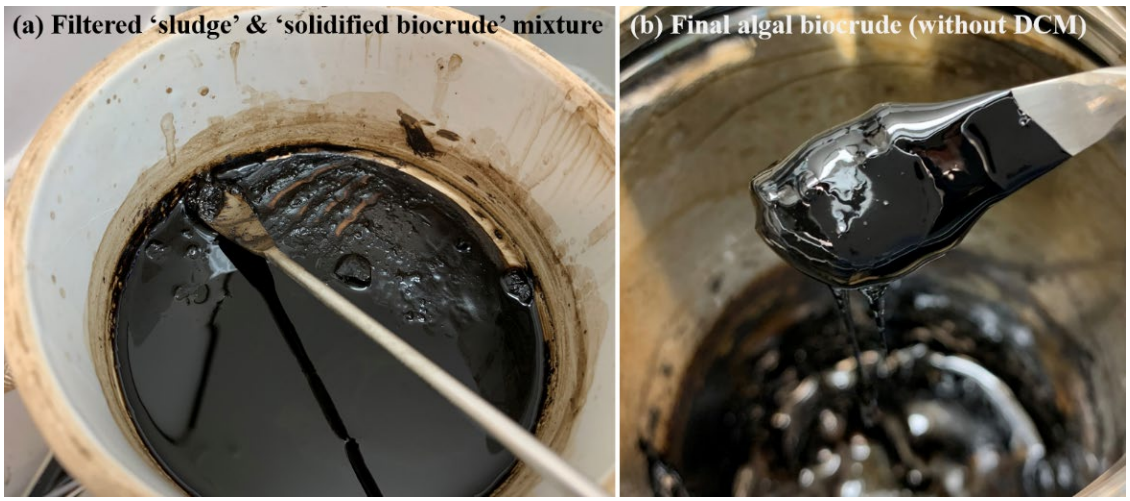

Figure 8. (a) Filtered product (sludge and solidified biocrude mixture) and (b) completed biocrude after evaporating DCM (dichloromethane).

Based on the optimized protocol, we calculated the yield rate of the monoculture and polyculture algae HTL reaction using the scale-up reactor. We analyzed a total of three sets of frozen algae, and an infected monoculture algae. Figure 9 shows the biocrude yield rate of each culture. The EFRI donation algae, which has been utilized to optimize our HTL and upgrading recipe, and the monoculture algae show around 2.4% biocrude yield rate based on the wet algae weight. The polyculture yield rate shows around 2.5 times higher than the other two cultures. The reason for the high yield rate of the polyculture algae is mainly due to the higher concentration shown in Figure 10. The last bar chart in Figure 9 is the result of the post-infected monoculture algae HTL yield rate, and the yield is reduced by

half compared to non-infected algae. In the processes of HTL and filtration, the post-infected algae show excessive sludges and rubber-like clumped algae shells compared to the normal algae.

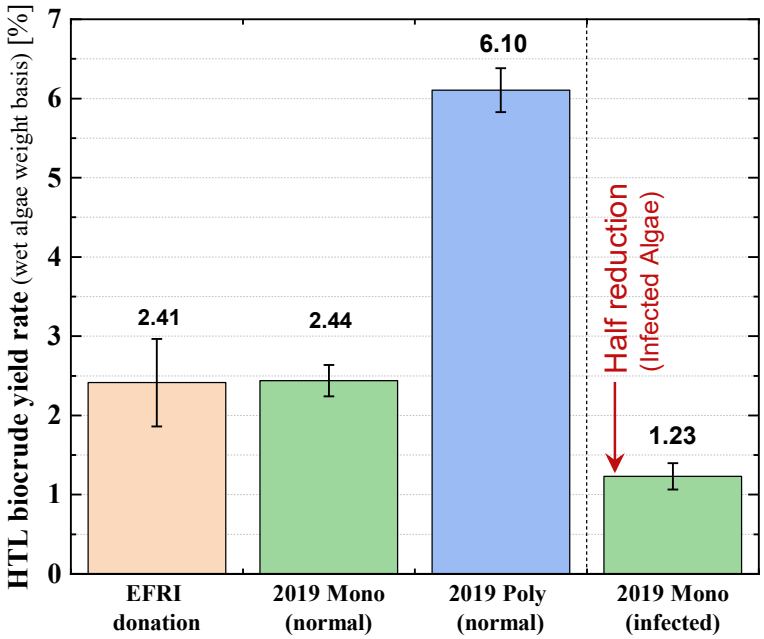

Figure 9. HTL biocrude yield rate comparison by algae cultures.

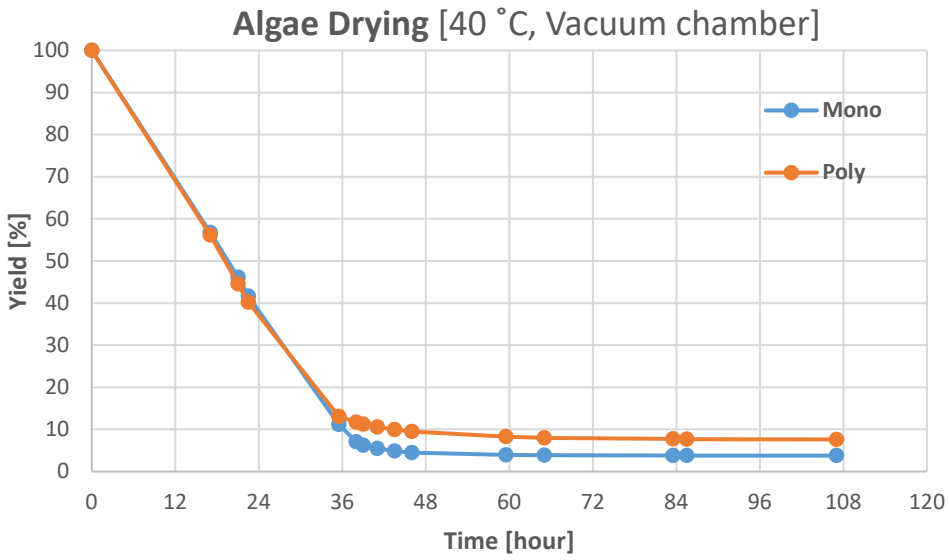

Figure 10. Mass yield profile for the wet mono and polycultures after drying under vacuum at 40 ˚C.

Another observation from the scale-up reactor HTL experiments is composition analysis of the three different algae cultures through GC-MS. Using the optimized HTL recipe (320°C + 30 mins, up to 350°C), the GC-MS analyses were completed for the EFRI algae and both mono- and poly-culture algae (EFRI algae are a large sample set from a previous NSF funded *Energy Frontiers Research Initiative* in which the performance of algal polycultures were established, and have provided additional algal samples for the project to work with). Biocrude compositions of the three algae groups are shown in Figure 11. To compare the biocrude compositions of the three algae groups, the GC methods including temperature rising rate and running times were kept the same. The top two figures (a) are the EFRI algae *(mixed culture)*, and left bottom two figures (b, d) are monoculture algae *(Selenastrum Capricornutum)* of different pond collection date, and the right bottom two figures (c, e) are polyculture algae *(Selenastrum Capricornutum, Chlorella Sorokiniana, and Scenedesmus Obliquus)*. The biocrude compositions are almost the same between the monoculture and polyculture, and the EFRI biocrude compounds were very similar to the mono and polyculture biocrude except a couple of long retention time species (47~48mins: e.g., $C_{17}H_{35}NO$, $C_9H_{16}O_4$, but negligible). And the top three species are identical to the small-scale microreactor GC-MS result. Also, the fungus infected (artificial infection) mono and polyculture algae biocrude compositions were identical to the non-infected algae.

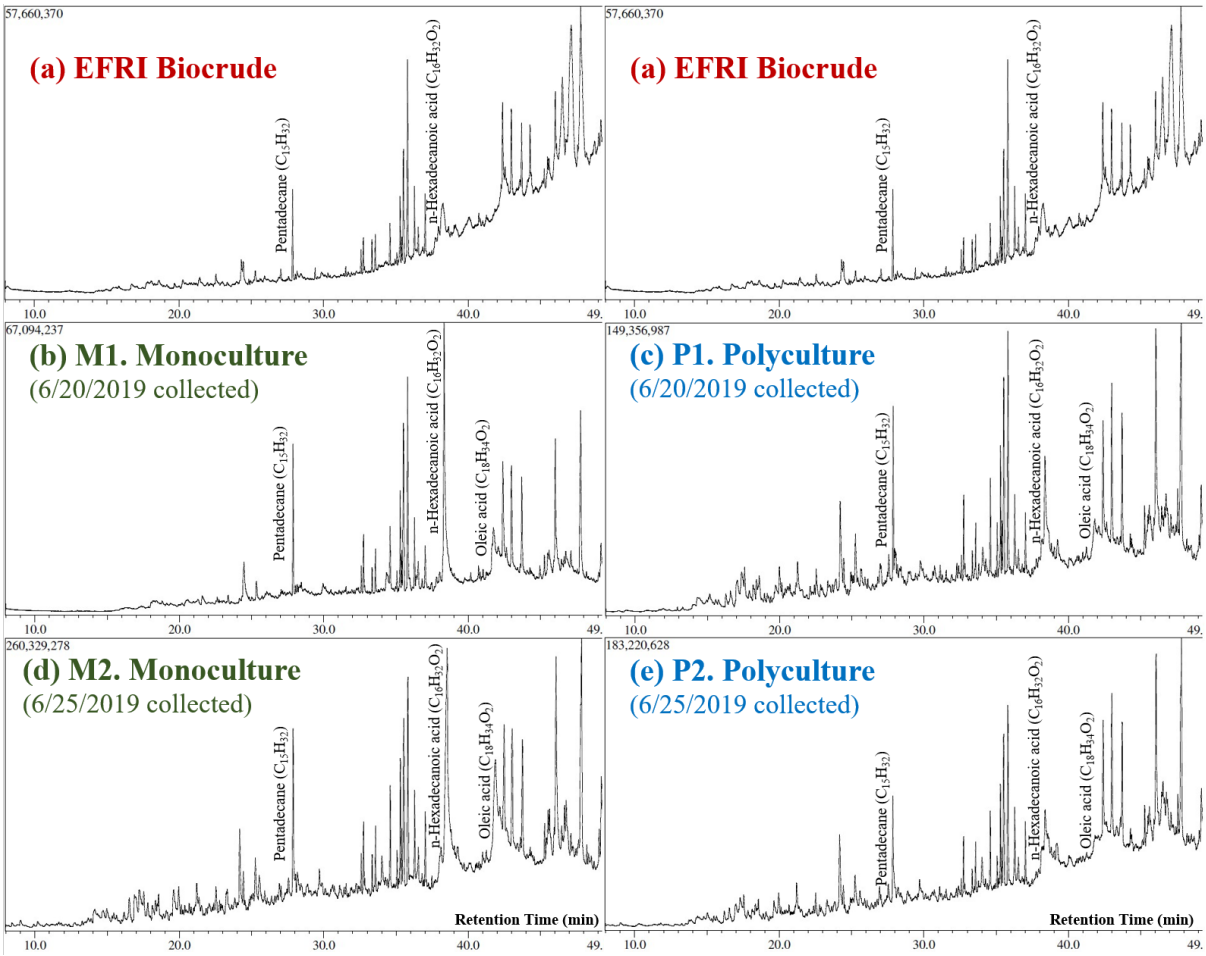

Figure 11: GC-MS analyses of compounds in the algal biocrude obtained from EFRI, Monoculture, and Polyculture algae: (a) EFRI algae, (b, c) Mono and Polyculture algae - 6/20/19 pond collected, and (d, e) Mono and Polyculture algae - 6/25/19 pond collected.

Figure 12 and Table 5 show the thermogravimetric analysis (TGA) and elemental analysis (CHON) of the HTL biocrude from monoculture and polyculture algae. In Figure 12, both mono and poly culture biocrudes show similar fuel-utilizable temperature ranges (up to 480°C) and slopes, but the polyculture biocrude contains more light hydrocarbon portion (up to 185°C, usually gasoline range) than the monoculture biocrude, and the polyculture biocrude has less residue than for the monoculture. This agrees with the elemental analysis of the dry algae (before HTL) and biocrude shown in Table 5.

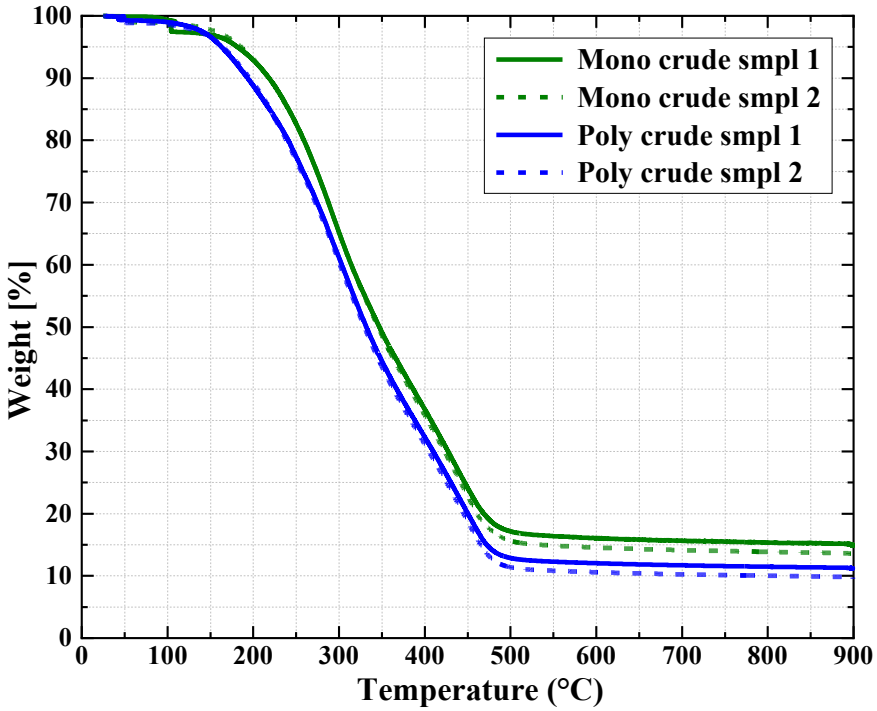

Figure 12. TGA analysis for mono and poly biocrude samples.

Table 5: Elemental analysis result for mono and poly biocrude.

Crude	C	H	O	N	HHV [MJ/kg]
Dry algae - Mono	47.34	6.99	38.33	7.34	20.68
Dry algae - Poly	52.10	7.35	32.14	8.41	23.46
Biocrude - Mono	74.76	9.41	10.61	5.22	37.26
Biocrude - Poly	76.06	9.55	9.37	5.02	38.09

Task 3. Life-cycle Assessment and Techno-Economic Analysis

We published a novel LCA that takes the temporally static GREET model developed by DOE and compliments that model with a submodel of algal feedstock production that is more biologically realistic, and which accounts for stochastic variation in algal growth that can occur due to temporally varying growth rates or crashes caused by disease [3]. We have updated that LCA with data from our 2019 demonstration project (see Task 1) that was performed in the 4.2-m^2 ponds at AzCATI. Discussions about this updated LCA were held with Troy Hawkins of Argonne National Lab and our team to review how our LCA/TEA approach [3] can integrate with other DOE life-cycle assessment efforts. Since our team's approach is based on the GREET model, developed by researchers at Argonne National Laboratory, our approach is compatible with the ongoing DOE efforts.

In addition to the existing LCA, we have worked to add fungal disease dynamics as a driver to the LCA. Elena will modify the submodel that feeds algal dynamics into GREET with a biologically realistic model of infection that accounts for how fungal disease can cause fluctuations and crashes of algae feedstock that limit their productivities [2]. Our hope was that the addition of biologically realistic equations and species interactions (e.g., disease) would improve reliability and realism of the GREET model output. Our analyses show that biological engineering of a multispecies consortium of algae has a greater positive impact on LCA metrics than chemical control of the fungal pathogen using a fungicide [2]. The DOE Algal Systems program has recently been reporting reduced GHG reduction potential for algae cultivation and conversion into fuels, with some pathways projected to reach a 50% GHG reduction [4]. The pathways explored in this project at such small scale do not approach this DOE BETO target. But the use of multispecies algae consortia shows the potential to maintain these target levels of GHG reduction when accounting for perturbation of algae productivity because of the impacts of disease, which will both increase the GHG emissions from algal fuel production and reduction energy return on investment (EROI) [2]. At the very least, this biological engineering approach will minimize the loss of EROI and increase of GHG emissions when compared to chemical treatment during algae cultivation.

We conducted a technoeconomic analysis (TEA) of a hypothetical chemical process to convert algal biomass to diesel fuel (and other product streams). We used process flow diagrams (PFD) adapted from published PNNL TEAs for hydrothermal liquefaction (HTL) of algae to biocrude and for subsequent upgrading of the crude bio-oil to fuels. We performed material and energy balances around the different unit operations in the proposed processes and used those results to determine characteristic sizes (e.g., surface area for a heat exchanger) that can then be used to estimate the capital cost for each piece of equipment using published cost correlations. Then, the total capital investment was estimated using a multiplying factor, per standard preliminary design procedures. Likewise, operating costs were estimated using textbook methods, which are based on rules of thumb and inputs for a few specific costs. All of these calculations were done via a dynamic simulation coded in Python. Ultimately, we were able to arrive at an estimate for the fuel selling price.

Figure 13 shows the PFD for the algae HTL facility. The algal biomass slurry is fed to the process and then pressurized and pumped through a heat exchanger for preheating, which also recovers thermal energy from the hot reactor effluent stream. The feed stream is heated further to the desired HTL temperature (300 °C in this analysis) in a subsequent heat exchanger with a heat transfer fluid as the heat source. The material enters the reactor where liquefaction occurs and the effluent stream is then cooled, the

pressure is let down, and solids are filtered out. The remaining material is then separated into an oil phase, an aqueous phase, and a gas phase.

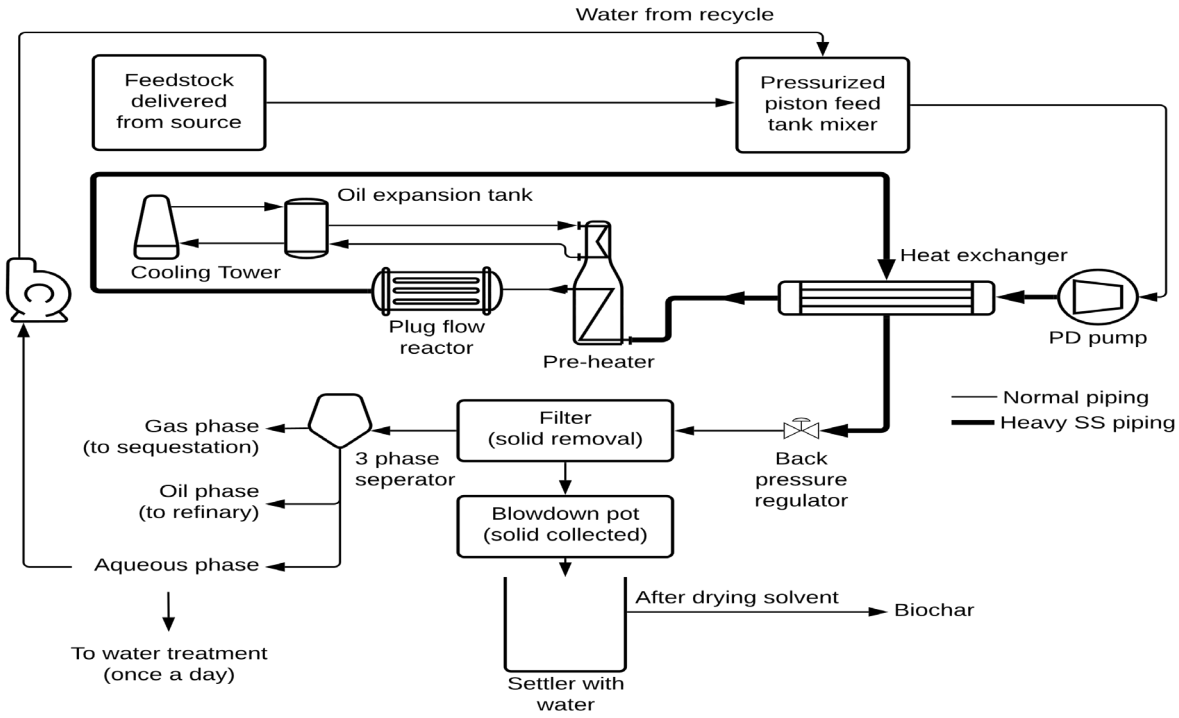

Figure 13: Schematic depiction of algae HTL process (adapted from PNNL report, [5])

Figure 14, which is from a PNNL report [5], shows a PFD for the biocrude upgrading facility. H_2 is added to the biocrude, and the stream is heated prior to entering the hydrotreater, where oil upgrading takes place. Thermal energy is recovered from the hot reactor effluent, which is cooled further in an additional heat exchanger and then enters a separation train to recover gases, aqueous products, gasoline, diesel, and heavier products that can be hydrocracked.

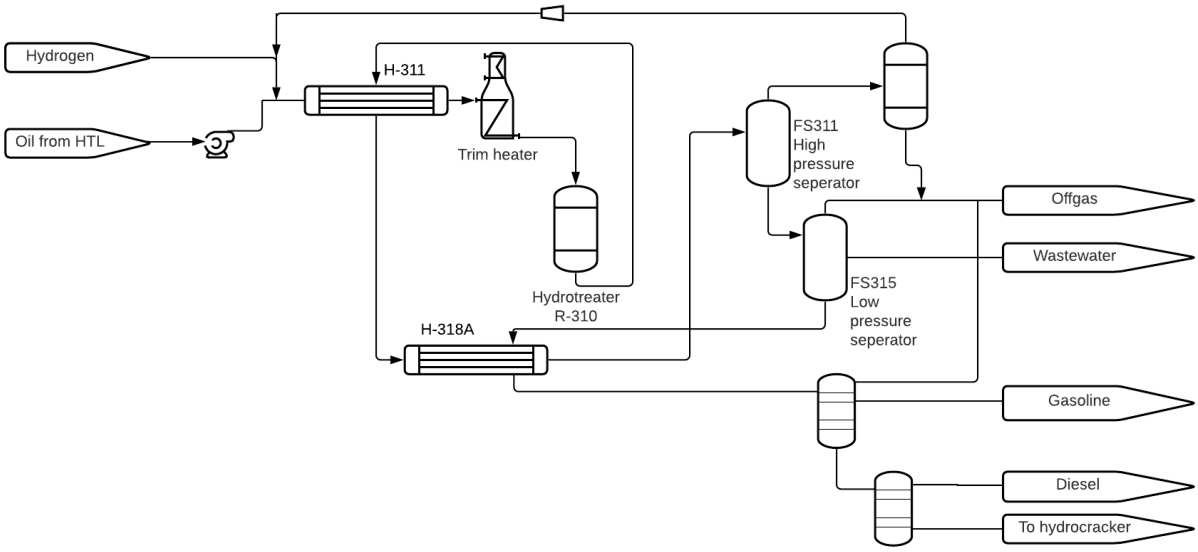

Figure 14: Schematic depiction of biocrude upgrading process (from PNNL report, [5])

We determined the fuel selling price for two distinct input data sets. One set (Case 1) used approximate values from the experimental work we did as part of this project and the other set (Case 2) was inputs from TEA studies done by PNNL, meant to represent operation at scale. The input that largely accounts for the large difference in fuel selling price is the cost of the algal biomass. This cost is much higher for our smaller scale, fixed term (six week) research study than it would be for producing algal biomass continuously at scale for production purposes.

Table 6: Summary of inputs and fuel selling price for two scenarios

	Case 1: This Project	Case 2: HTL at scale
Feedstock cost ($/kg dry biomass)	25,000	0.086
Feed rate (tons/day)	476	1340
Feedstock loading (wt% biomass in slurry)	6	20
Biocrude yield from HTL (wt% dry basis)	26	59
Baseline diesel cost ($/gal)	635,000	2.76

Task 4. Biocrude Upgrading to Tailored Fuels

Upgrading studies with actual HTL biocrude were performed in microreactors at the bench scale to screen several commercial catalysts finalize the procedures to use in the scale-up reactors. The biocrude oil from HTL is not suitable for use as a fuel. Additional processing is needed to remove heteroatoms (e.g., N, O). We tested ten different catalysts for upgrading the crude bio-oil. Experiments were done in mini-batch reactors under hydrogen pressure. Using the literature as our guide, we selected operating conditions of 400°C at 70 bar hydrogen pressure with 20 wt% catalyst loading (relative to mass of crude bio-oil). Each run was performed in triplicate. Table 7 gives the experimental results.

Table 7: Elemental composition (wt %) of upgraded oil and mass and energy recoveries after upgrading.

	Yield [wt %]	**C** [wt %]	**H** [wt %]	**N** [wt %]	**O** [wt %]	**HHV** [MJ/kg]	**Energy Recovery** [%]
HTL Biocrude (pre-upgrading)	-	68.92	8.53	4.64	17.91	32.45	-
1 Pt/C	5.92	69.94	7.22	7.54	15.67	31.45	5.75
2 Ru/C	9.54	62.94	7.72	1.30	28.04	28.07	8.25
3 Pd/C	5.66	49.23	8.51	0.96	41.30	22.68	3.95
4 Ni/C	42.30	81.20	10.52	2.73	5.55	40.33	52.6
5 Activ. Carbon	21.20	74.20	9.23	1.53	15.04	35.24	23.0
6 Pt/Al_2O_3	39.60	79.57	10.11	3.57	6.75	39.20	47.8
7 Ru/Al_2O_3	41.10	79.05	9.78	4.04	7.13	38.62	49.0
8 Pd/Al_2O_3	62.10	78.22	10.15	2.76	8.87	38.49	73.67
9 Ni/SiO_2-Al_2O_3	57.30	81.29	10.46	3.45	4.80	40.42	71.43
10 No catalyst	73.70	76.82	9.85	3.96	9.37	37.67	83.58

The carbon materials gave low recoveries of upgraded oil, which led to low energy recoveries. It is possible that these materials were acting more as sorbents than catalysts and capturing molecules of interest. The metals on alumina supports performed better, but the Ni catalyst on silica-alumina gave the highest value for the HHV of the upgraded oil. This catalyst and Pd on alumina were the only ones to give energy recoveries exceeding 70%. Hence, these are the most promising materials for upgrading the bio-oil. Even these materials, however, did not reduce the O and N content to the low levels desired for a finished fuel. Some additional upgrading would likely be needed. The oil yields from upgrading with the noble metals on carbon are all less than 10 wt%, which was unexpected. The rest of the mass of the original HTL biocrude was recovered in the gas and solid phases. Overall mass balances were always around 100%, indicating that all of the original biocrude mass was being recovered and accounted for in the products from the upgrading reactions. The O and N content in the upgraded oils exceeded those in the original biocrude for the upgrading runs with these three noble metal catalysts supported on carbon. We have no good explanation for this unexpected outcome, but note that the very low upgraded oil yields here mean the upgraded oil retained only a small fraction of the O and/or N in the original HTL biocrude. The large majority of the O and N atoms went to either the solid products or the gaseous products.

We analyzed the upgraded oil samples through GC-MS to separate and identify molecules in each sample. Table 8 lists the compounds in greatest abundance (by area %) in each sample. These molecules are largely hydrocarbons, and they correspond only to that portion of the upgraded oil that would be sufficiently volatile to elute from a GC column. The GC-MS results also revealed the presence of compounds containing O and N atoms, as expected from the elemental analysis results. Many of these compounds contained multiple heteroatoms. These mini-batch reactors have guided the definition of the catalyst and reaction conditions to implement in the scale-up reactors.

Table 8: Compounds in greatest abundance in upgraded oil samples.

Compound	**#1**	**#2**	**#3**	**#4**	**#5**	**#6**	**#7**
1. Pt/C	Chamazulene	Dodecane, methyl-	Hexadecane, tetramethyl	Naphthalene, trimethyl	Eicosane	Methanonaphthalene, dihydro methyl ethylidene)-	Trimethyl azulene
	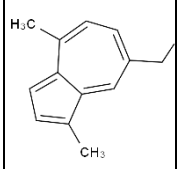	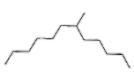	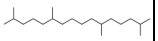		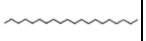	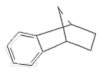	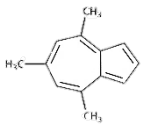

2. Ru/C	Octadecane	Pentadecane	Chamazulene	Hexadecane, tetramethyl-	Naphthalene, tetramethyl-	Naphthalene, trimethyl-	Naphthalene, trimethyl-
			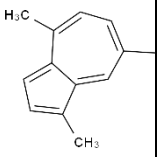		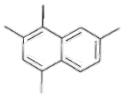		
3. Pd/C	Hexadecane, tetramethyl-	Heptadecane	Tetramethyl naphthalene	Nonacosane	Octacosane	Dodecane, 2-methyl-8-propyl-	Pentadecane
	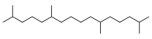		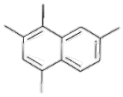			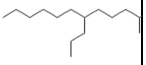	
4. Ni/C	Eicosane	Hexadecane	1-Heptanol, 2-propyl -	2-Methyltetracosane	Pentacosane	Heneicosane	Pentadecane, trimethyl-
			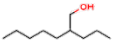				
5. Activated carbon	Eicosane	Heptadecane	Hexadecane, tetramethyl-	Tridecane	Pentacosane	Pentadecane	Methyl 7,9-tridecadienyl ether
			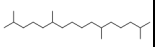				
6. Pt/Al_2O_3	Octadecane	Pentadecane	Hexadecane, tetramethyl-	Nonadecane nitrile	Hexadecane	Pentacosane	Heptadecane nitrile

		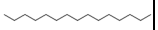	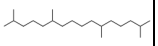	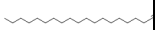	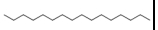	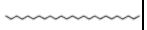	
7. Ru/Al_2O_3	Heptadecane nitrile	Eicosane	Hexadecane, tetramethyl-	Pentadecane	Octadecane nitrile	Hexadecane	Heneicosane
			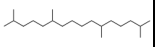		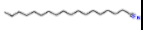		
8. Pd/Al_2O_3	Eicosane	Heptadecane	Hexadecane, tetramethyl-	Octadecane	Hexadecane	Heneicosane	Pentadecane, trimethyl-
			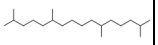				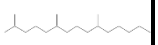
9. Ni/SiO_2-Al_2O_3	Heptadecane	Pentadecane	Hexadecane	Octadecane	Hexadecane, tetramethyl-	Pentadecane, trimethyl-	Octacosane
					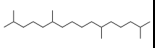		
10. No catalyst	Pentadecane	Heptadecane	Hexadecane, tetramethyl-	Hexatriacontane	Pentadecane, trimethyl-	Dodecanedioic acid, 2TBD MS derivative	Octacosane
			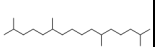	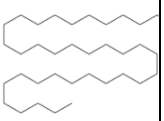		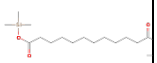	

Transition to Scale-Up Reactors

We have finalized the catalyst based on the microscale reactor results in Tables 7 and 8. Among the best yield rate catalysts (#8, #9 catalyst), the Ni/SiO_2-Al_2O_3 catalyst showed the highest hydrodeoxygenation efficiency, so we selected the Ni/SiO_2-Al_2O_3 and 350°C, and we varied catalyst loading rates (2 ~ 20 w%) and reaction times (1 ~ 4 hours). The reaction time was selected to be 4 hours which showed best viscosity rate, and the catalyst loading rate was determined based on the composition results. Figure 15 shows the boiling point basis fuel type differences of the three catalyst rates. Diesel (between 240 and 350°C), gasoline (lower than 185°C), and jet (between 185 and 240°C) fuel portions are gradually increased with catalyst rate due to promoted cracking rate of longer chain hydrocarbons. So, the heavy gas oil portion (between 350 and 570°C) is reduced by adding more catalyst. Figure 16 indicates the functional groups of the biocrude and upgraded biofuels with different catalyst rates. Biocrude deoxygenation was sufficiently done with a 2 percent catalyst rate (especially -C=O- and -C-O-), and the upgrading reaction significantly promoted the hydrocarbon saturation (-C=C-). Based on these results, we selected the optimized upgrading recipe to the catalyst loading 10% and 4 hours reaction.

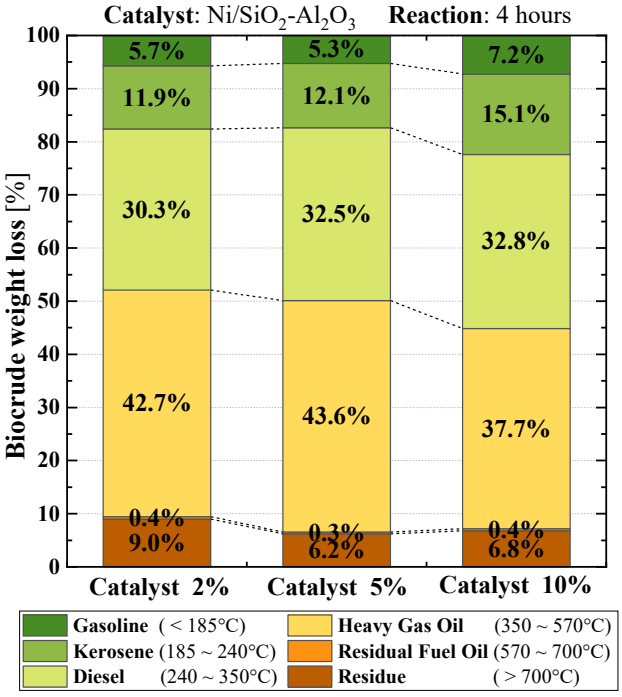

Figure 15. Boiling point basis fuel types of upgraded biofuels with different catalyst rates (2, 5, 10 wt%, 4 hours reaction)

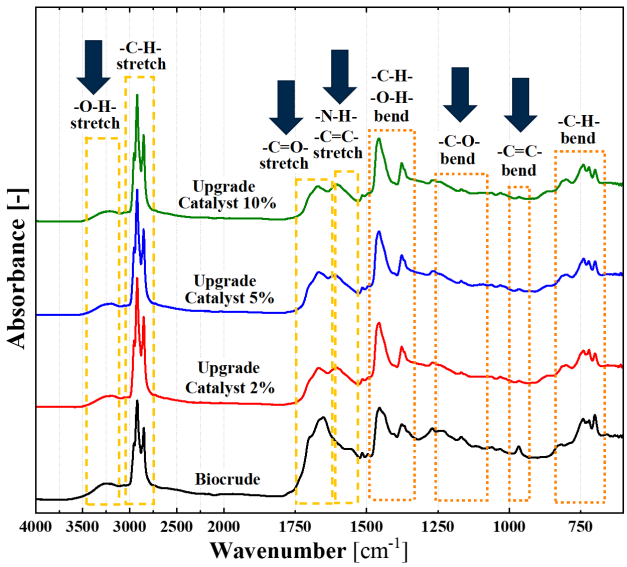

Figure 16. FTIR spectra showing the functional groups present in algal biocrude and upgraded biofuels with different catalyst rates (2, 5, 10 wt%, 4 hours).

The post-upgrading algal biofuel GC-MS results and top components (highest catalyst loading rate: 20 w%) are shown in Figure 17 and Table 9. The highest catalyst loading case shows that more than half species are n-alkane, and the top species are pentadecane and heptadecane. The total alkane components in the biofuel are 69.9%, and the averaged carbon numbers are 17.03 for this recipe.

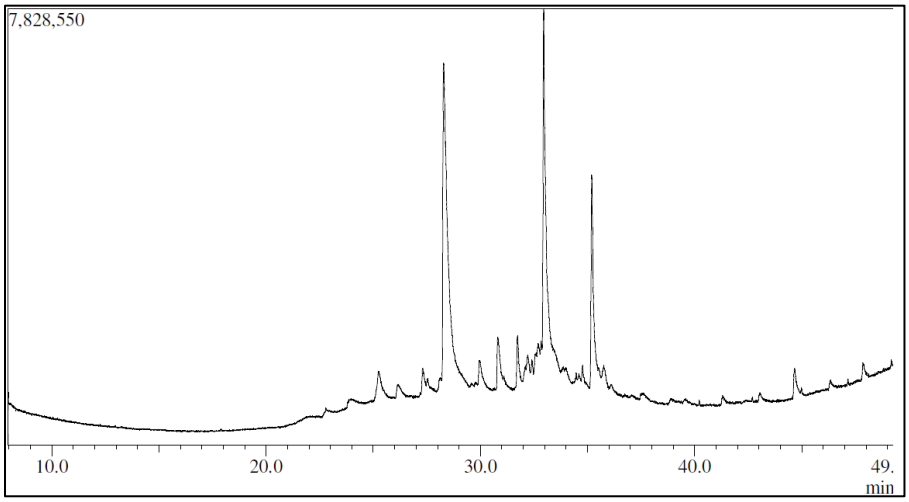

Figure 17: GC-MS analysis of compounds in the upgraded biofuel from EFRI biocrude.

Table 9. Top 21 species of EFRI algae biofuel (covers over 88.3% species).

R.Time	Area%	Area% Sum	Name	Formula
28.279	27.12	27.12	Pentadecane	$C_{15}H_{32}$
32.956	20.87	47.99	Heptadecane	$C_{17}H_{36}$
35.200	8.83	56.82	Eicosane	$C_{20}H_{42}$
34.768	4.26	61.08	Acetic acid, 3,7,11,15-tetramethyl-hexadecyl ester	$C_{22}H_{44}O_2$
33.397	3.60	64.68	Ethyl 5-(chloromethyl)-2-oxooxolane-3-carboxylate	$C_8H_{11}(Cl)O_4$
29.963	2.51	67.19	Pentadecane, 2-methyl-	$C_{16}H_{34}$
31.735	2.40	69.59	Pentadecane, 2,6,10-trimethyl-	$C_{18}H_{38}$
32.699	1.83	71.42	8-Heptadecene	$C_{17}H_{34}$
25.264	1.73	73.15	Hexadecane, 2,6,10,14-te tramethyl-	$C_{20}H_{42}$
33.990	1.71	74.86	Nonyl octacosyl ether	$C_{37}H_{76}O$
32.208	1.61	76.47	1-Decanol, 2-hexyl-	$C_{16}H_{34}O$
44.664	1.47	77.94	Dotriacontane	$C_{32}H_{66}$
32.595	1.39	79.33	Pentadec-7-ene, 7-bromo methyl-	$C_{16}H_{31}(Br)$
33.863	1.37	80.70	Formic acid, dodecyl ester	$C_{13}H_{26}O$
32.407	1.34	82.04	Oleyl alcohol, trifluoroacetate	$C_{20}H_{35}(F_3)O_2$
32.838	1.20	83.24	1-Nonadecene	$C_{19}H_{38}$
32.097	1.16	84.40	Cyclohexanecarboxylic acid, 4-hexyl-, 2,3-dicyano- 4-(pentyloxy)phenyl ester	$C_{20}H_{24}(N_2)O_3$
27.312	1.09	85.49	2,6,10-Trimethyltrideca ne	$C_{17}H_{36}$
35.517	0.99	86.48	1-Dodecanol, 3,7,11-tri methyl-	$C_{15}H_{32}O$
31.103	0.94	87.42	Cyclooctasiloxane, hexadecamethyl-	$C_{16}H_{48}O_8(Si_8)$
28.123	0.89	88.31	9-Octadecene, (E)-	$C_{18}H_{36}$

The upgraded algal biofuel compositions were valuable enough to utilize in powertrain systems, but the physical property (i.e., viscosity) was not enough to directly put into the powertrain fueling systems (e.g., diesel engine). So, we developed two methods to apply the final fuel into the fueling systems.

The first method was phase separation (centrifuging) of the algal biofuel with *n*-hexadecane mixture (50:50 wt%). The fuel physical condition was successful (ready to use condition), and Figure 18 shows a picture of the upgraded biofuel after phase separation.

Figure 18. Upgraded algal biofuel with *n*-hexadecane (50:50 v%) after phase separation.

The second method was distilling the algal biofuel based on the temperature. The distilled fuel physical condition was also successful (ready to use condition), and Figure 19 is a picture of the distilled algal biofuel for the mixed algae sample from cultivation of the polyculture (left is gasoline range and right is diesel/kerosene range). Figure 20 shows a functional group analysis of the distilled algal biofuel for the mixed algae (polyculture) sample. As shown in the peaks, the compositions were almost identical to the pre-distillation upgraded biofuel.

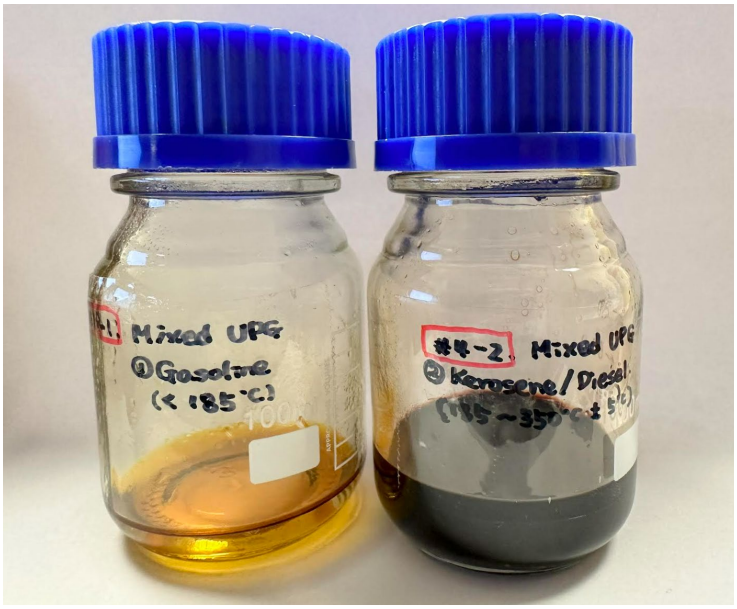

Figure 19. Distilled algal biofuel by temperature (Gasoline <185°C & Kerosene/Diesel 185~340°C).

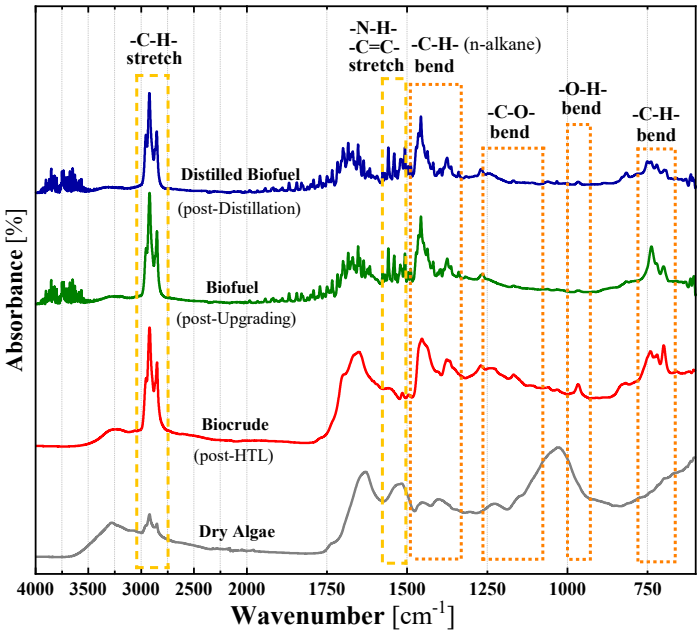

Figure 20. FTIR results of the distilled algal biofuel.

Analyses of the sample of upgraded, distilled, algal bioblendstock for MCCI combustion were performed by staff at the National Renewable Energy Laboratory. We were not able to meet the 500 ml target of bioblendstock, but around 130 ml of sample was produced (100 ml from an algal polyculture and 30 ml from an algae monoculture), which is an adequate amount for the property analyses given the techniques used at NREL. Results are summarized in Table 10. As mentioned above, the algae species that yielded the distilled upgraded bioblendstock sample were for the monoculture *Selenastrum capricornutum* and for the polyculture *Selenastrum capricornutum*, *Scenedesmus obliquus*, and *Chlorella sorokiniana*.

The outcomes of the fuel property analyses show a reasonable density and cloud point for both blendstocks, a somewhat high viscosity (diesel range is 1.4 to 4.0 according to the ASTM D975 specification) and a somewhat low heating value. Blended at 30% into a diesel basestock that is well within D975, these blendstocks would yield a fuel with properties falling well within D975 requirements. The normalized sooting tendency, measured by Aurora Xiang and Dr. Charles McEnally of Yale University. The sooting tendency is compared to No. 2 diesel fuel, and normalized against the signal from No. 2 diesel fuel. The NSC represents a relative soot concentration by volume, and is calculated by the following formula. The sooting tendcy is reduced versus No. 2 diesel fuel by 35 and 40% for the polyculture and monoculture-derived fuel samples, respectively.

$$NSC = \frac{LSSR_{test\ fuel} - LSSR_{undoped}}{LSSR_{diesel} - LSSR_{undoped}}$$

Table 10: Fuel Property Analyses for the Distilled Upgraded Biocrude Samples from a Mixed Polyculture and a Monoculture.

Fuel Property	Mixed Algae Sample (100 ml)	Mono Algae Sample (30 ml)
Density at 20°C (g/cm^3)	0.882	0.912
Viscosity at 40°C (mm^2/s)	5.04	5.42
Cloud Point	-2.5°C	-11.9°C
Higher Heating Value (MJ/kg)	30.52	35.54
Lower Heating Value (MJ/kg)	27.88	33.17
Indicated Cetane Number (ASTM D8183)	39	-
Normalized Soot Concentration (-)	0.66	0.59
Elemental Composition, C wt.%	81.1	46.9
Elemental Composition, H wt.%	12.5	11.2
Elemental Composition, N wt.%	3.4	6.0
Elemental Composition, O wt.% (diff)	3.1	35.9

These measurements of fuel properties and composition were complicated by challenges with sample stability, several months after the upgrading and distillation processes. A clear layer formed which was almost certainly a layer of water, that had been absorbed by the fuel during cooling after distillation. As a consequence the normalized sooting tendency is listed in the table above from the fuel fraction of the separated products.

Nonetheless, the fuel samples generated by the project team achieved the objective of remaining within general characteristics of diesel fuel, retaining a reasonable heating value and lower sooting tendency. The fuel samples showed a reasonable cloud point, but a lower cetane number that a typical diesel fuel.

Overall, the outcomes show that further improvements in the upgrading process are needed to obtain an algal bioblendstock that approaches the qualities that made the model algal bioblendstocks (represented by *n*-hexadecane in 30 vol.% blends and by renewable diesel fuel as a neat fuel) so successful in improving MCCI combustion and yielding substantial potential for improvements in engine brake thermal efficiency, as shown in the next section of this report.

Additional study – Lipids extraction for diesel

In addition to the biocrude upgrading process, we carried out the lipid extraction experiments using the Soxhlet device towards the lipid mixture hydrodeoxygenation process shown in Figure 21. The algae sample is dried in the heated vacuum chamber at a high temperature (65 $^{\circ}$C) first, and the dry algae is crushed before the extraction process. Figure 22a shows the Soxhlet lipid extraction device. We tested several solvents to verify the most effective lipid extraction with the polyculture algae. Figure 6b shows the extracted lipids with 12 hours of extraction (a) and the lipid-out dry algae (b) that can be further utilized for pyrolysis and biochar production. The extracted lipids condition was the best with n-hexane solvent and the highest yield rate was methanol solvent case (>15% w%). In follow-on work, we performed experiments to determine the best solvent for lipid extraction and conducted upgrading experiments through the hydrodeoxygenation process.

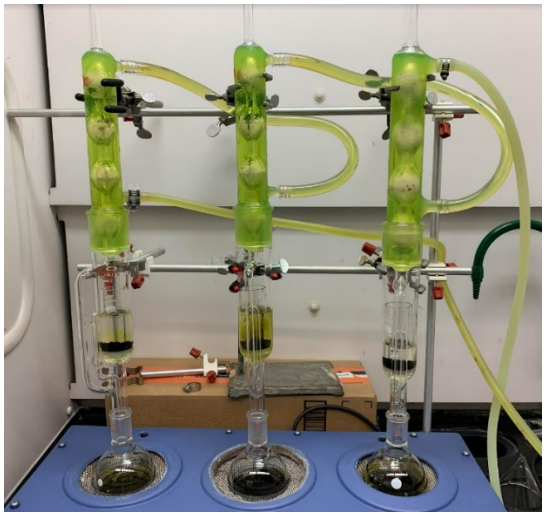

Figure 21: Soxhlet lipid extraction apparatus for dry algae.

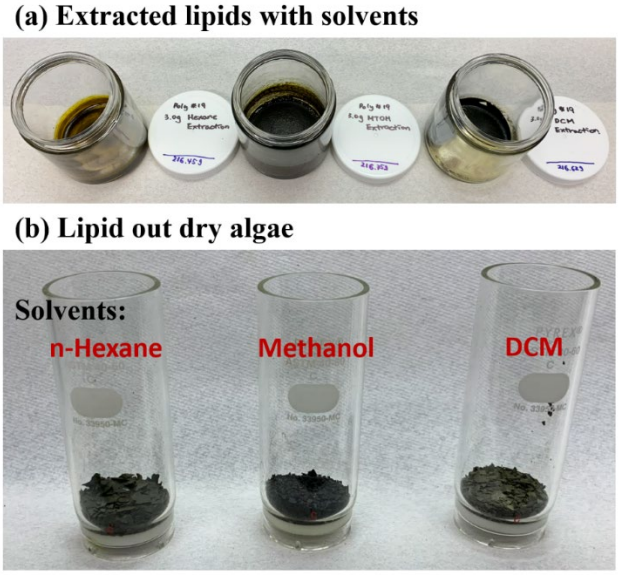

Figure 22: Soxhlet lipid extraction results.

We carried out lipid extraction and upgrading experiments. We tested 4 solvents and two combined solvents and decided on the best two solvents: n-hexane and Folch method (Chloroform and Methanol mixture). As Figure 23 shows, the Folch method solvent showed a significantly higher yield rate than the *n*-hexane solvent, but the Folch extracted lipid condition is darker and stickier. Table 10 shows the elemental analysis results of both solvents. The Folch extraction still contains unexpected contents (e.g., nitrogen) and less heating value than the *n*-hexane solvent. So, we focused on the *n*-hexane solvent for upgrading pure components with a transesterification stage.

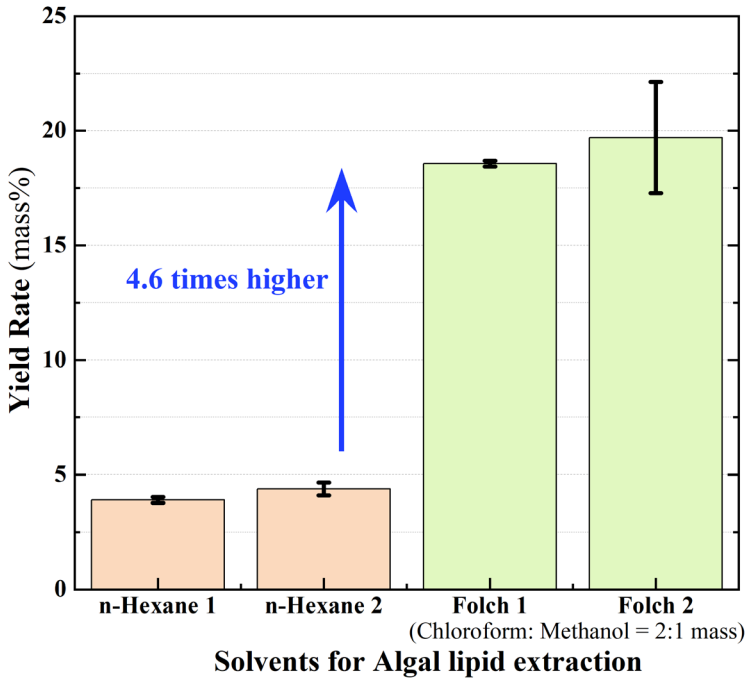

Figure 23. Lipid extraction yield rate comparison by mass.

Table 10: Elemental analysis result for extracted lipids and lipids upgrading.

Crude	C	H	O	N	HHV [MJ/kg]
Lipid Extr: *n*-hexane	78.04	11.31	10.08	0.57	41.77
Lipid Extr: Folch	65.66	9.36	21.31	3.67	32.94
Lipid Upgrading: Folch	68.72	9.90	17.21	4.17	35.21

We carried out the lipid extraction quality assessment with two solvents: Folch (methanol and chloroform mixture) and *n*-hexane. Figure 24 shows the elemental composition differences of the biocrude, extracted lipids with Folch and *n*-hexane solvents. Folch solvent extraction showed better yield rates than *n*-hexane solvent, but it showed higher oxygen and nitrogen contents and lower heating values. Figure 25 indicates the boiling points basis fuel types of the biocrude and extracted lipids from Folch and *n*-hexane solvents. The *n*-hexane solvent extraction showed a higher purity level which

contains over 90% of valuable components, such as triglyceride and fatty acids range, and a lower amount of solid residue.

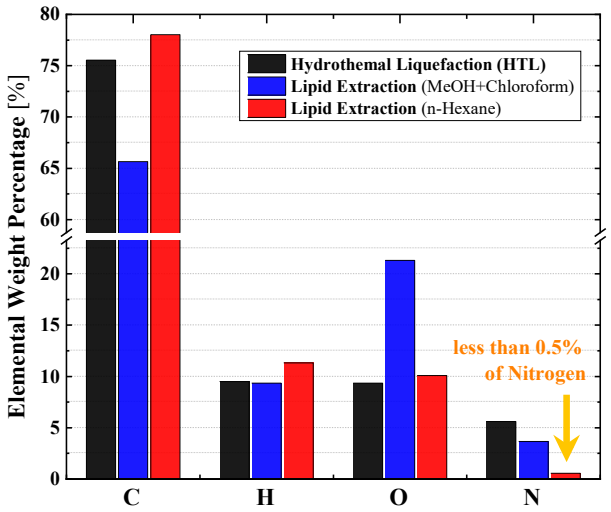

Figure 24. Elemental composition comparisons between HTL biocrude and extracted lipids by Folch and *n*-hexane solvents.

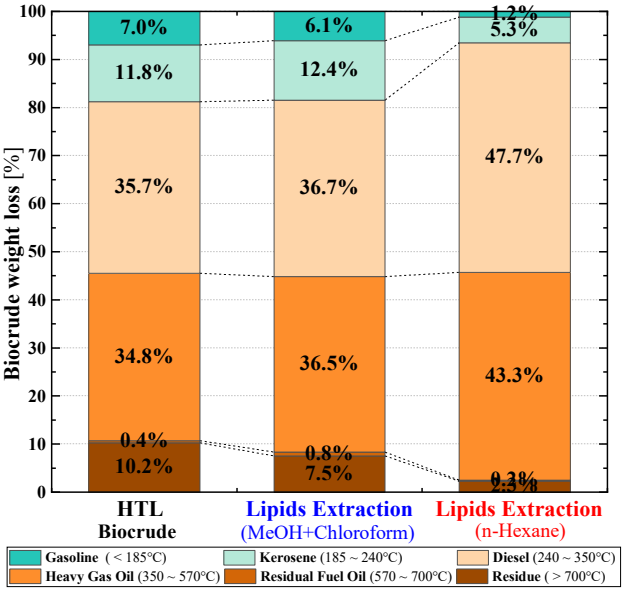

Figure 25. Boiling point basis fuel types of biocrude and extracted lipids by Folch and *n*-hexane solvent.

The objective in the lipid extraction study described in this section was to understand the yield differences between HTL of whole algae versus a lipid extraction strategy. The former, HTL, has the potential for better mass and energy efficiency on a life cycle basis, but the processing and upgrading can be complicated. Whereas with lipid extraction, the yields are lower, but the upgrading is very straightforward. As a late addition to the project plan, (i.e., outside the scope of the SOPO), we did not perform a comparison of the lipid route versus the whole algae HTL route in terms of LCA or TEA.

Task 5. Engine Studies and Simulation

In support of advanced combustion processes and improving MCCI combustion is having good reactivity under dilute and over-mixed mixture conditions. To compare a potential pathway for the algal fuel production, wherein we remove all heteroatoms and yield a mixture of saturated bio-hydrocarbons, we evaluated the ignition response to dilution. We compared an ultra low sulfur diesel fuel, with a synthetic Fischer-Tropsch fuel and a sample of Renewable Diesel fuel. As a consequence, to explore the potential of algal bioblendstocks to optimize fuel properties to improve MCCI combustion, we have used this renewable diesel sample as a model for an upgraded algal fuel. Figure 27 shows that the renewable diesel fuel sample is just as dilution tolerant as the Fischer-Tropsch fuel. These initial measurements tie together the efforts under Task 2-5, and are the basis on this project's reliance on HTL of algae to produce biocrude and hydroprocessing of the biocrude to an algae-derived bioblendstock.

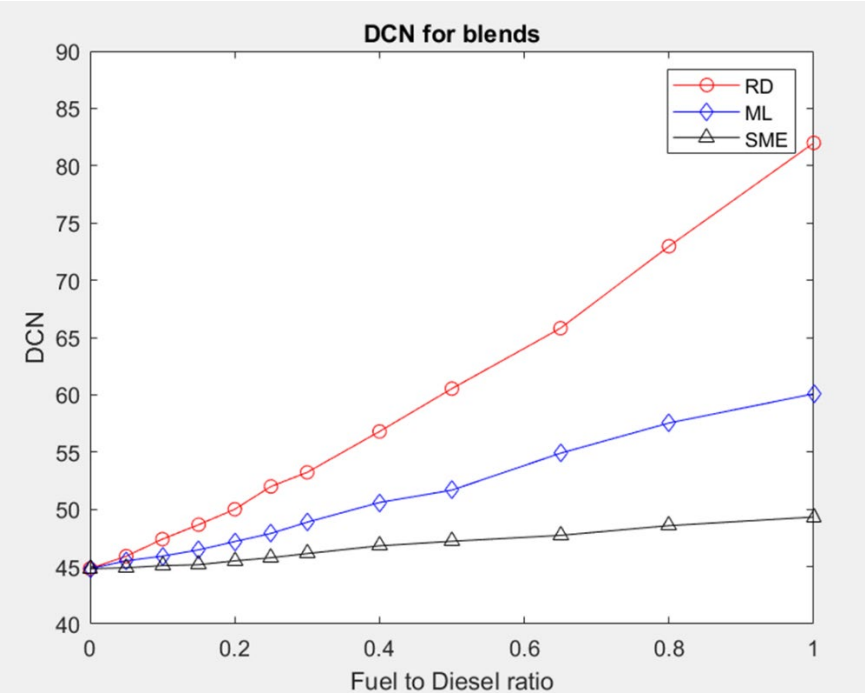

Figure 26. Derived cetane number (DCN) measurements of blending renewable diesel (RD), methyl laurate (ML) and soybean methyl ester (SME) into an ultra low sulfur diesel fuel. At 20 and 30 vol.% addition, blending with RD yields substantial improvements in DCN by $\geq$ 5 points.

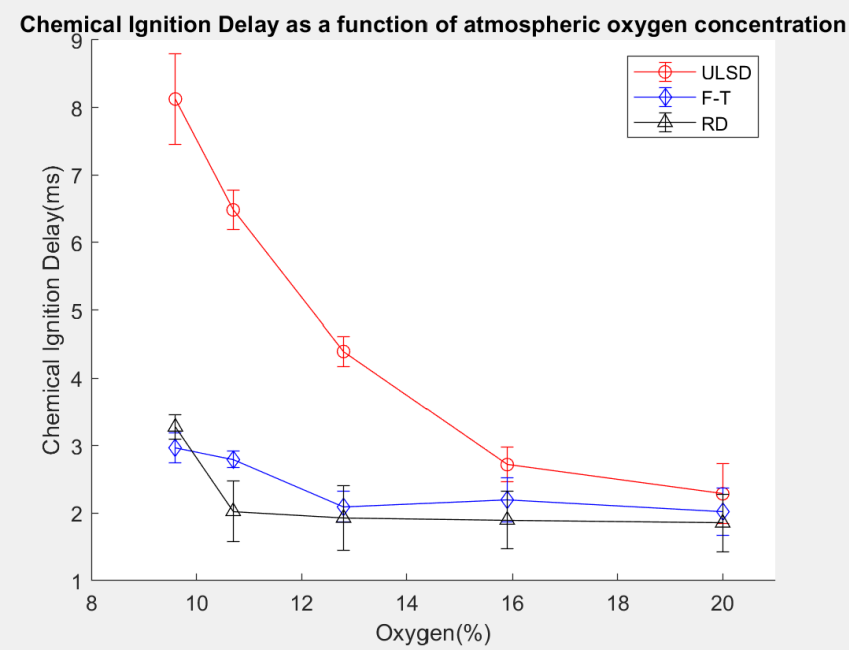

Figure 27. Diluted chemical ignition delay measurements for renewable diesel (RD), Fischer-Tropsch and an ultra low sulfur diesel fuel, showing dilution tolerance of the saturated alternative fuels.

Smoke point measurements (using an ASTM standard smoke point lamp) were performed to examine how blending with esters (short chain methyl laurate and convention soy methyl ester biodiesel) compared with blending with a long chain alkane dominated sample of renewable diesel fuel. While methyl laurate provided the greatest increase in smoke point (meaning lowered sooting tendency) when blended into a conventional petroleum diesel fuel, the renewable diesel fuel gave greater increase in smoke point than the soy methyl ester. This outcome confirmed the choice of processing strategy – to seek to produce alkane-rich biohydrocarbons and eliminate oxygen content to achieve a stable bioblendstock that provides the opportunity improve MCCI combustion by both reducing sooting tendency and increasing ignition quality.

Due to limitations in availability of algal bioblendstock material to perform engine experiments, an early step in the project was to examine the potential primary species that would be present in an optimized algae-derived fuel. Early examinations of biocrude composition, showed an abundance of octadecenoic acid and hexadecanoic acid, as shown below. On this basis, the fuel property, engine and simulation studies focused on *n*-hexadecane as a model for the algal bioblendstock. Moreover, focusing on a single molecule to represent the algal bioblendstock streamlined the application of chemical kinetics to simulate autoignition and engine combustion, and allowed for a detailed examination of available reaction kinetics mechanisms.

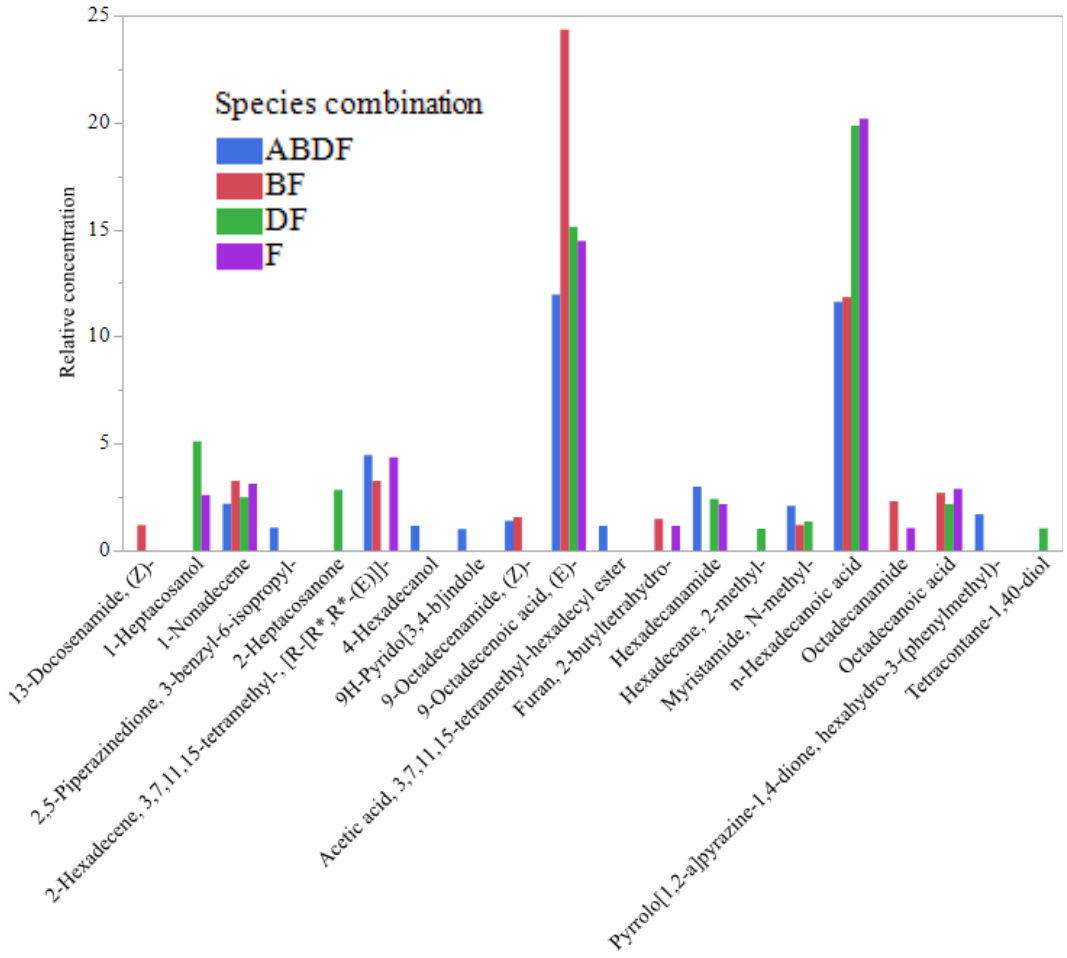

Figure 28. Compounds that comprise >1% of concentration. Biocrude composition, from a representative sample from the NSF EFRI project for monoculture and polyculture samples, appears to be high in C18:1 and C16:0 with the relative concentration of each differing by species combination. Minor compounds include alkanes, amides, fatty alcohols, aldehydes and other fatty acids.

Thus to simulate blending behavior of the algal bioblendstock, we have relied on *n*-hexadecance as a surrogate for experimental and numerical studies. In engine studies, this has meant blending *n*-hexadecane into diesel fuel at up to 30 vol.%. In comparison, experiments with neat renewable diesel were performed to represent adoption of a 100% renewable fuel to represent a practical algal biofuel to replace diesel fuel. Optimization of MCCI combustion was explored for both *n*-hexadecane blends and 100% renewable diesel fuel.

What follows is a summary of scope, methodology and key outcomes from the combustion chemistry and engine optimization studies.

Simulation Studies

Simulation efforts focusing on the ignition behavior of single- and multiple-component fuels. This included testing of detailed chemical mechanisms for key individual species of interest (primarily large straight-chain and branched-chain alkanes), identification of more "CFD-friendly" (~100-200 species) reduced chemical mechanisms from the literature for key species and for various diesel surrogate blends, simulations of the CFR engine including comparisons with experimental data, and simulations of a heavy-duty diesel engine using meshes available from an earlier DOE SuperTruck project to explore how best to take advantage of algae-derived fuels. We have collaborated with Dr. Charlie Westbrook on improving detailed mechanisms to capture the ignition behavior of large branched-chain alkanes under low-temperature-combustion conditions. Separate work performed at the University of Michigan has shown failures of existing large alkane mechanisms to capture observed ignition behavior in the CFR engine, through studies of ignition behavior of jet fuel surrogates [6]. Data from Cheng was provided to Dr. Westbrook to assist in mechanism improvements.

Understanding low- and intermediate-temperature heat release and ignition behavior has been a primary focus of the simulation work, and was major subject explored by J. Han who was a doctoral student supported by this project [7]. Toward that end, simulations of the CFR engine operating in HCCI mode continued for various fuel mixtures for which experimental data are available, and tools were developed to extract insight into the species and reactions involved in low- and intermediate-temperature heat release. Examples for a three-component RON 80 mixture of n-heptane, iso-octane, and ethanol are shown in Figures 29 and 30. There results from three different chemical mechanisms (A62, R178, and A1121, where the number indicates the number of species considered) are compared for an intake pressure of 1 bar. In Figure 29, experimental and simulated in-cylinder pressure-temperature trajectories are plotted together with cumulative heat release for a condition that corresponds to the critical compression ratio (CCR $\approx$ 11, for this condition). Large differences are evident among the three chemical mechanisms.

The pressure-temperature trajectories are then imposed in a zero-dimensional CHEMKIN model to perform reaction pathway analyses. These provide insight into the species and reaction pathways that are active in low-, intermediate-, and high-temperature heat-release phases. An example of the different species and pathways involved in the breakdown of iso-octane in the three-component RON 80 mixture at different temperatures for the A62 mechanism is shown in Figure 30. This information, combined with comparisons of computed and measured key intermediate species, provides insight into potential areas of improvement for the reduced chemical mechanisms that are needed for CFD simulations of practical engine configurations.

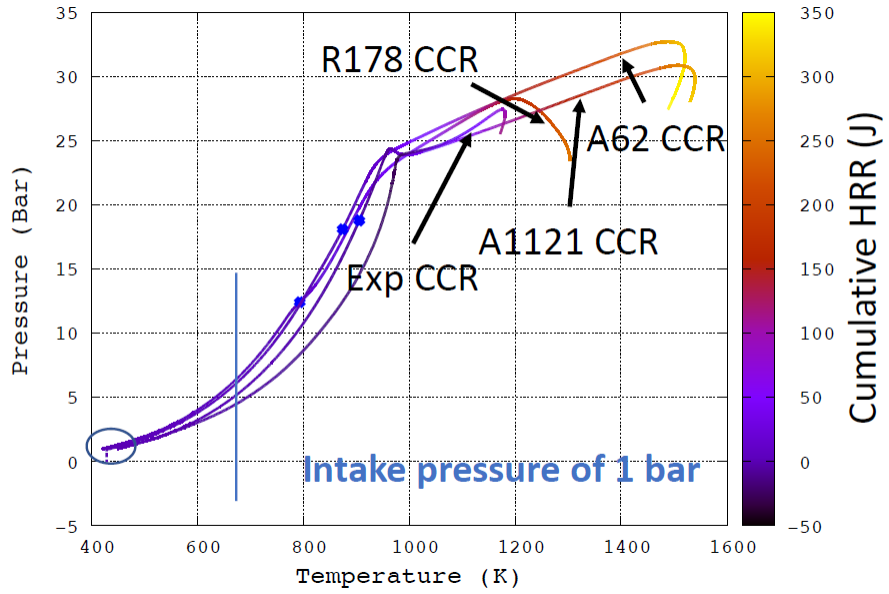

Figure 29. Examples of measured and computed pressure/temperature/heat-release trajectories in the CFR engine.

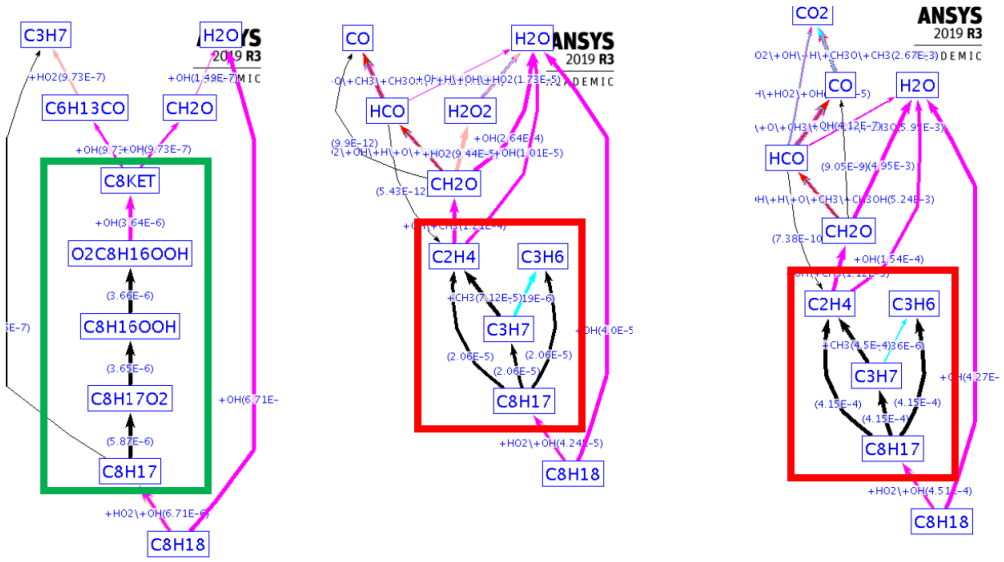

Low-Temperature regime of 750 K **intermediate-Temperature regime of 900 K** **High-Temperature regime of 1100 K**

Figure 30. Examples of reaction pathway analyses in low-, intermediate-, and high-temperature stages of heat release. For the low temperature pathways, the graphic emphasizes the multistage oxygen addition and internal isomerization steps.

An example of the challenges with capturing the low temperature ignition behavior is shown below, in an attempt to capture the critical compression ratio trend as a function of intake air temperature in the modified CFR engine.

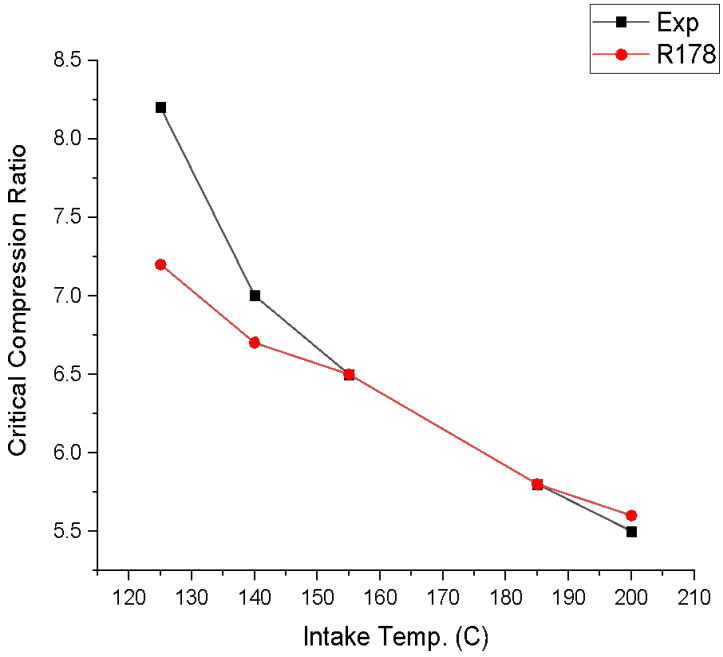

Figure 31. Comparison of CCR measurements and simulations for 100% *n*-hexadecane (C16) at 4 different intake temperatures of 125°C, 140°C, 155°C, 185°C, and 200°C. Evaluated multizone model and reaction kinetics, showing relatively similar CCR at higher intake temperatures, but a discrepancy at lower temperatures intake temperatures where low temperature reaction kinetics play a stronger role.

Follow up studies have used UM's multizone model and our GC-MS system to produce comparisons of the ignition behavior of *n*-hexadecane and *n*-octadecane against existing kinetic models, particularly those that Dr. Jun Han's simulations showed to be the most promising. That work continues beyond the conclusion of this project, and will be the subject of a future publication.

Simulation also included parametric studies of the Volvo 13L engine, demonstrating that the ability to capture the influence of fuel composition on soot formation and potential efficiency improvements that could be realized by taking advantage of the physical and chemical properties of algae-derived fuels. To that end, two engine operating conditions were identified for the 13L engine. For each operating condition, simulations were performed for conventional diesel fuel and for diesel fuel with a high percentage of large n-alkane molecules, to look for evidence of efficiency improvement.

The CFD model of a constant-volume high-pressure combustion chamber was exercised to explore the ignition and sooting behavior of two large n-alkane molecules (n-dodecane and n-hexadecane) under diesel-engine-relevant conditions. The extent to which unresolved turbulent fluctuations influence the results was determined by comparing results from a model that accounts for turbulent fluctuations (a transported probability density function – tPDF – method) with one that ignores them (a locally well-stirred-reactor – WSR – model). The largest influence of turbulent fluctuations was found to be in the soot predictions, which were in better agreement with experiment for the tPDF model. Differences between n-dodecane and n-hexadecane results were found to be small. There is some evidence from

the literature that it may be possible to take advantage of differences between the physical and chemical properties of these two molecules in an engine to realize nonnegligible differences in efficiency and soot levels. However, more sophisticated gas-phase chemistry and soot models may be needed to capture the subtle differences in CFD modeling [7].

Fuel Ignition and Composition Studies

We have performed dosing studies of *n*-hexadecane and *n*-octadecane into practical diesel fuels to explore changes in key fuel ignition parameters, such as the critical equivalence ratio, which is a measure of EGR tolerance [8]. To permit the operation of the CFR octane rating engine on real, full boiling range diesel fuels, the heavy end of the diesel fuel (>T90) needed to be removed from the fuel so that it can be vaporized into the CFR engine intake. In past work, this was done to enable studies of both conventional diesel fuels and the FACE diesel fuels [8,9]. To accomplish the removal of the >T90 fraction, we configured a distillation apparatus to generate these diesel fuel cuts. We verified that CN has not been appreciably altered by performing this distillation, as in our past work [8,9]. Due to the pandemic, there were problems with acquiring the components for our distillation apparatus, after some delays, we were able to purchase and receive the final components. We performed some initial distillation trials to obtain the <T90 fraction for some of the Marathon diesel fuel for the bench scale ignition studies. Concerns about overheating the fuel during distillation (our initial >T90 fractions have been discolored after distillation) led to development of an upgraded distillation apparatus (Fig. 32 b) to perform vacuum distillation on the baseline diesel fuel, the performance of which was verified GC-MS/FID analyses on the original fuel and distilled fractions from the distillation.

We also operated a highly instrumented derived cetane number instrument (CID510 cetane analyzer) and (after much delay related to the pandemic) perfected the methods and application of the auxiliary oven on our GC-MS/FID system for improved analysis of combustion intermediates. We performed the critical compression ratio, critical equivalence ratio and combustion intermediates analyses for comparison with simulation efforts at both UM and Penn State (which contributed to the completion of the doctoral thesis by Jun Han at PSU [7]).

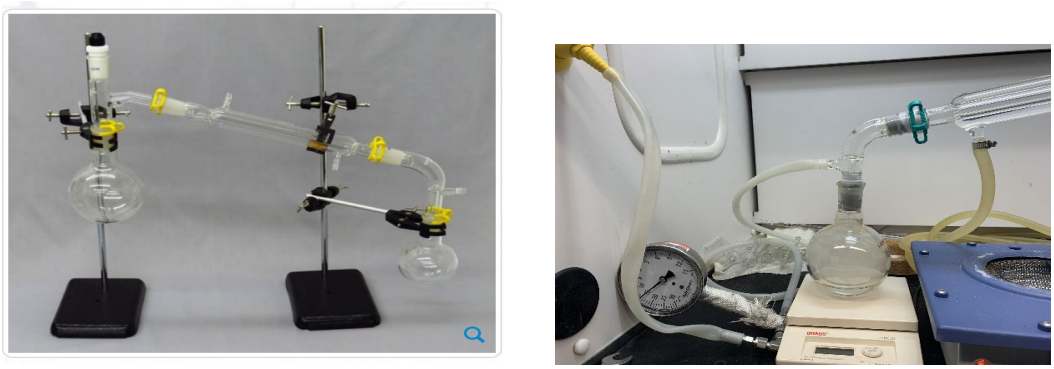

(a) (b)

Figure 32. (a) Picture of a generic distillation apparatus that has served as the basis for the design of a new distillation system prepared at UM to process full boiling range diesel fuels for use in the CFR octane rating engine for autoignition studies by removing the >T90 fraction, (b) initial design of the UM

vacuum distillation apparatus for removing >T90 fraction of diesel fuel, and applied to the distillation of the upgraded algal biocrude into gasoline and diesel fractions.

A drum of n-hexadecane was acquired for CFR engine and multi-cylinder engine experiments and 30 drums of Marathon brand diesel fuel were acquired to provide a consistent baseline diesel fuel through the duration of the project. The baseline Marathon diesel fuel has also been characterized in our Derived Cetane Number instrument, the CID510, using ASTM Method D7668.

Fuel	ID (ms)	CD (ms)	DCN
Marathon Diesel	3.5428	5.1989	46.66

Marathon performed a suite of fuel composition and property analyses. The tables below show some of the results provided by Marathon staff.

UDescr

Sample Point Description SPDescr			**U of M Project, Baseline Diesel**
Analysis	Component	UoM	
Cetane, CID Derived, ASTM D7668	Derived Cetane Number		49.6
D5773, Cloud Point, (C/F)	Automated Cloud Point, F	deg. F	-22
D93A, Flash, (C/F)	Flash Point, F	deg. F	152
Bromine Number, UOP304	Bromine Number	gBr/100g	0.29
D4176, Workmanship	Determination		Pass
D3338, Net Heat of Combustion	Net Heat of Comb.(In.-Lb. Units), S corr	BTU/lb	18577
Lubricity, by HFRR, D7688	Lubricity	um	470
Aromatic Hydrocarbon Types in Aviation Fuels and Petrleum Distillates, D6379	Mono-Aromatic Hydrocarbons	vol. %	6.3
Aromatic Hydrocarbon Types in Aviation Fuels and Petrleum Distillates, D6379	Di-Aromatic Hydrocarbons	vol. %	0.7
Aromatic Hydrocarbon Types in Aviation Fuels and Petrleum Distillates, D6379	Total Aromatic Hydrocarbons	vol. %	7
D5949, Pour Point	Pour Point, F	deg. F	-36
D1319, FIA Hydrocarbon Types	Aromatics	vol. %	7
D482, Ash	Mass of Ash	g	0.0031
Biodiesel Content by NIR	% Biodiesel	vol. %	0
D4052, Density/Gravity/SpGrav	Sp. Grav at 60F		0.8362
D4052, Density/Gravity/SpGrav	Density at 15.6C	g/cc	0.8354

D4052, Density/Gravity/SpGrav	API Gravity (calculated)	deg. API	37.7
D2887, Distillation, Simulated	D86 IBP (predicted)	deg. F	354
D2887, Distillation, Simulated	D86 Recovered 5% (predicted)	deg. F	394
D2887, Distillation, Simulated	D86 Recovered 10% (predicted)	deg. F	407
D2887, Distillation, Simulated	D86 Recovered 20% (predicted)	deg. F	427
D2887, Distillation, Simulated	D86 Recovered 30% (predicted)	deg. F	445
D2887, Distillation, Simulated	D86 Recovered 50% (predicted)	deg. F	477
D2887, Distillation, Simulated	D86 Recovered 70% (predicted)	deg. F	514
D2887, Distillation, Simulated	D86 Recovered 80% (predicted)	deg. F	535
D2887, Distillation, Simulated	D86 Recovered 90% (predicted)	deg. F	566
D2887, Distillation, Simulated	D86 Recovered 95% (predicted)	deg. F	593
D2887, Distillation, Simulated	D86 FBP (predicted)	deg. F	625
D2887, Distillation, Simulated	D93 Flash Point (predicted,calc)	deg. F	157
D5453, Sulfur	Sulfur, Average	ppm (wt.)	1

Sample Description	U of M Diesel
Sample Date	4/18/2021
wt%	
Saturates	92.98
Paraffins	27.09
Monocycloparaffins	18.41
Dicycloparaffins	31.15
Tricycloparaffins+	16.33
Aromatics	7.02
Monoaromatics	6.26
Alkylbenzenes	2.27
Naphthenebenzenes	2.40
Dinaphthenebenzenes	1.59
Diaromatics	0.09

Naphthalenes	0.09
Acenaphthenes, Dibenzofurans	--
Fluorenes	--
Triaromatics	0.13
Phenanthrenes	0.13
Naphthenophenanthrenes	--
Tetraaromatics	--
Pyrenes	--
Chrysenes	--
Pentaaromatics	0.53
Perylenes	--
Dibenzanthracenes	0.53
Thiopheno Aromatics	--
Benzothiophenes	--
Dibenzothiophenes	--
Naphthobenzothiophenes	--
Unidentified Aromatics	--
Class II	--
Class III	--
Class IV	--
Class V	--
Class VI	--
Class VII	--
Groups (wt%)	
Total Cores	2.82
Monoaromatics	1.67
Diaromatics	0.12
Triaromatics	0.17
Tetraaromatics	--
Pentaaromatics	0.86

Over a period of two quarters, the distillation apparatus was modified to accommodate vacuum distillation to bring down the boiling temperature range for the baseline distillation. In the initial trials, a significant amount of vapor loss was experienced because of the vacuum suction and less time for the vapors to condensate. Even after the installation of a graham condenser to allocate more time for condensation, volume balance of the distilled and distillate was not achieved. This also resulted in a mismatch between the GC-MS/FID comparative analysis with the baseline diesel fuel. Hence, to minimize the vapor losses, a further modification was made by using an antifreeze liquid to condensate the distilled vapors rapidly. This helped to significantly reduce mass loss. This approach was successful

and so we proceeded with the cetane number testing and applying it in the CFR engine to study autoignition properties.

Figure 33: Upgraded vacuum distillation apparatus to accommodate low-temperature condensation of vapor distillate

The GC-MS/FID analysis of the distilled diesel was also observed to agree with that of the baseline diesel. After this validation, almost 1.5 gallons of marathon baseline diesel was distilled and examined in CFR engine experiments, i.e., studying the critical compression ratio, and critical equivalence ratio sweeps for the baseline diesel as well as 30% n-Hexadecane blended diesel. The DCN test was performed to study how much the fuel composition was been changed and the difference was negligible considering the variability of the results of the derived cetane testing instrument i.e., CID. Below are the results from the CID.

Fuel	ID (ms)	CD (ms)	DCN
Marathon Diesel	3.5428	5.1989	46.66
Distilled Marathon Diesel	3.6085	5.3033	45.97

Work on the CFR engine and the GC-MS/FID coupled to the engine has been applied to the study of autoignition of n-hexadecane at 155°C and 1 bar intake temperature and pressure, respectively. Attached is a sample chromatogram with numerous peaks detected by FID and identified by the MS. To avoid running the full boiling diesel through the GC-MS, we have identified the mixture ratio for normal and iso-cetane to achieve a comparable DCN and have it act as a simulated diesel fuel. In work that will extend beyond the completion of this project, we will repeat earlier experiments of CR sweeps along with the GC-MS/FID for this simulated diesel and then blending this with 30% n-hexadecane to represent fuel A30. These results will be simulated using the UM multi-zone model of the CFR engine and the kinetic models that Dr. Jun Han's simulations showed to be the most promising.

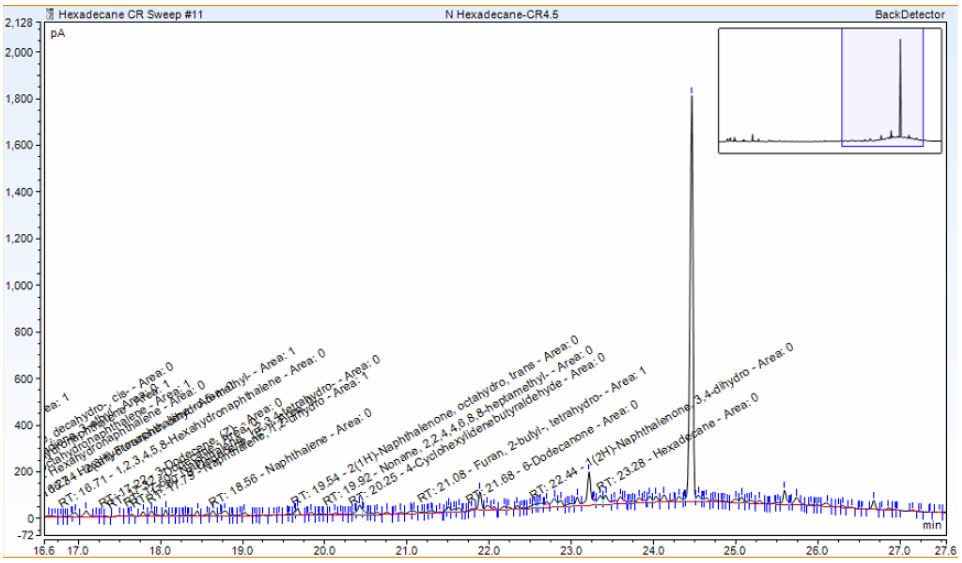

Figure 34: a sample chromatogram of n-hexadecane at compression ratio 4.5

Engine Experiments

The engine experiments performed in the final quarters of the project were comprised of two phases as described below:

1) An experimental matrix of four points has been finalized which include the low speed and high speed combined with the low load and high load test conditions to understand the overall trends which will then further help us in understanding the effects of the biofuel blending (phase 2). We performed baseline experiments and optimized a select set of engine operating parameters (injection strategy parameters, boost level, EGR%) on the Marathon baseline diesel fuel.
2) After having the results for the baseline diesel fuel, Phase 2 involved running the model compounds which represent the upgraded algae biocrude (c.f., *n*-hexadecane) blended with the baseline diesel fuel to achieve engine optimization for increased efficiency and decreased GHG emissions.

The design of experiments method was used for the efficient planning and determination of exact testing conditions. Instead of the "sweep" test planning for the multiple independent variables, a more robust and rather efficient method of "space-filling" was used. This method is used to fill up the n-dimensional input variable space with the least number of combinations of the input variables. The industry standard ASCMO software package guided this design of experiments. For the given input parameters, ASCMO sets a set number of data acquisition points to model the impact of those input parameters. Once the "screening experiments" of low and high speed and load combination experiments are completed, the next data acquisition points were obtained using ASCMO with the given input parameters of rail pressure, injection duration, start of injection, and for the blended fuels, the blending ratio.

Light-Duty Engine Studies

For the Phase 1 of Task 5, the engine mapping for the 1.9L engine being used in this study was finalized. Ideally, the entire range of operating points in the real world like scenarios should be considered for the optimization purposes however, several factors limited the range of speed and load conditions that are actually being tested. These factors include the frequency of the condition that is being desired by the drivers on the road, the range over which the current engine setup could produce reliable and trustworthy (steady state and repeatable) results, the limitations of the current setup, and lastly among these conditions, those experimental points were selected which were closer to already higher efficiencies. The test point being tested for the speed/load benchmarking are 1750 rpm and 2300 rpm for the low and high speed respectively and 60 Nm and 110Nm for the low and high load respectively as shown in Figure 35 (reprinted from [10]) these points are marked in triangles as A, B, C, and D.

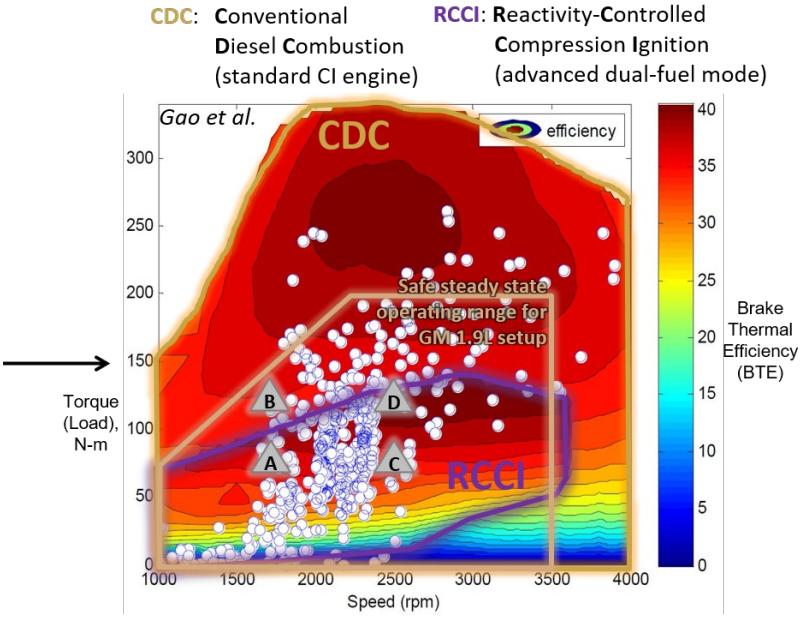

Figure 35: Benchmarking test point selection for speed/load based on typical duty cycles (from [10]).

Initial benchmarking tests for the baseline diesel yielded the following brake thermal efficiencies and the corresponding smoke numbers for the aforementioned speed load test points.

Test points	BTE (%)	Smoke Number	NOx (g/kWh)	EGR Fraction (%)	PM 2.5 (ug/m3)*
A	35	0.644	1.06	17.78	0.7
B	38	2.107	1.57	12.20	1.1
C	34	0.489	1.60	13.24	0.54
D	38	1.795	1.965	10.10	0.5

As per the expectations, high load points B and D are better off with the brake thermal efficiency at 38% as compared to 34% and 35% for low load points C and A, respectively. In the next stage, either of these points B and D will be selected for further optimization using the space-filling industry scale software, ASCMO, and through controlling various critical parameters that will help us in pushing the efficiency beyond the baseline benchmark followed by the target of reducing GHG emissions without losing the higher efficiency.

For the optimization process, 65 points test matrix was developed by ASCMO followed by the baseline testing. These test points were based on 5 different independent variables being main injection duration and timing, pilot injection duration and timing, and intake boost pressure. The desired output parameters, for the optimization process, were 110 Nm of torque and increased BTE with reduced emissions. This was achieved with the help of only the optimization process alone and without using any blending of algal biofuel model compound as shown in plots below. The suggested points from ASCMO helped us achieve a slight (2.5-3%) increase in BTE and a significant decrease in FSN, as shown in Fig. 36. The optimization process helped in achieving reduced THC as well, from 0.24 g/kWh to 0.12 g/kWh. However, an increase in NOx was observed from 1.50 g/kWh to 2.83 g/kWh.

The next step in the process was to study the effects of blending algal-based biofuel model compounds, n-Hexadecane in this scenario. A 30% blending ratio was chosen based on its effectivity shown from previous studies. A similar approach, as used in the previous step, was used to utilize ASCMO for the optimization using hexadecane blends. The final results seemed promising as we were able to achieve slightly higher BTE, unlike the previous studies which have shown a slight dip in BTE because of the reduced heating content of biofuels. A maximum increase of 3% from the original baseline and 0.8% from the optimized-without-algal biofuel baseline was achieved for BTE. It must be noted that at the first optimized test point, a maximum increase in BTE was observed however, this point resulted in maximum NOx. To counter the NOx, an increase in intake EGR was used from 4% to 11%. This resulted in a 0.48% reduction of BTE however, the effect on NOx was quite significant, as can be seen in Fig 39.

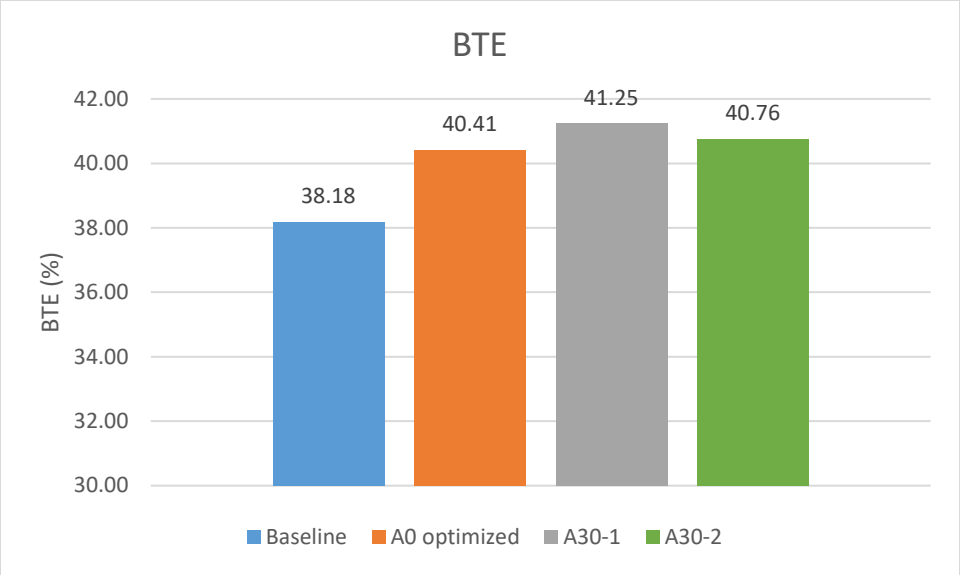

Figure 36: An increase of 2.4% in BTE can be observed for A0 and 3.07% for A30 optimized test point 1. The former was achieved solely through optimization by varying control parameters whereas, the latter one was achieved through both, 30% biodiesel blend and optimization process.

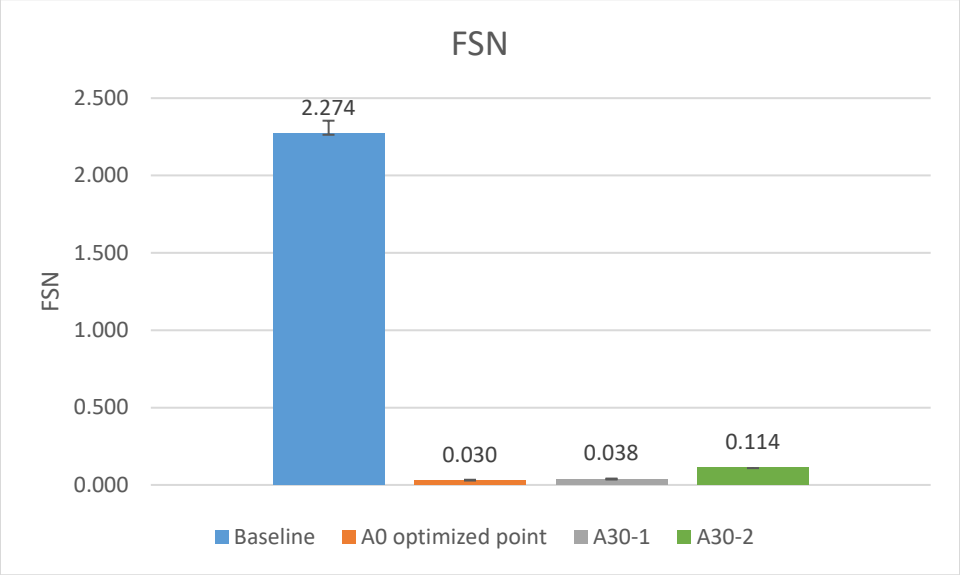

Figure 37: This plot shows that a significant reduction in FSN can be achieved through engine optimization without even using the A30 blend. Moreover, A30 seems to cause a slight increase in FSN but that is not significant.

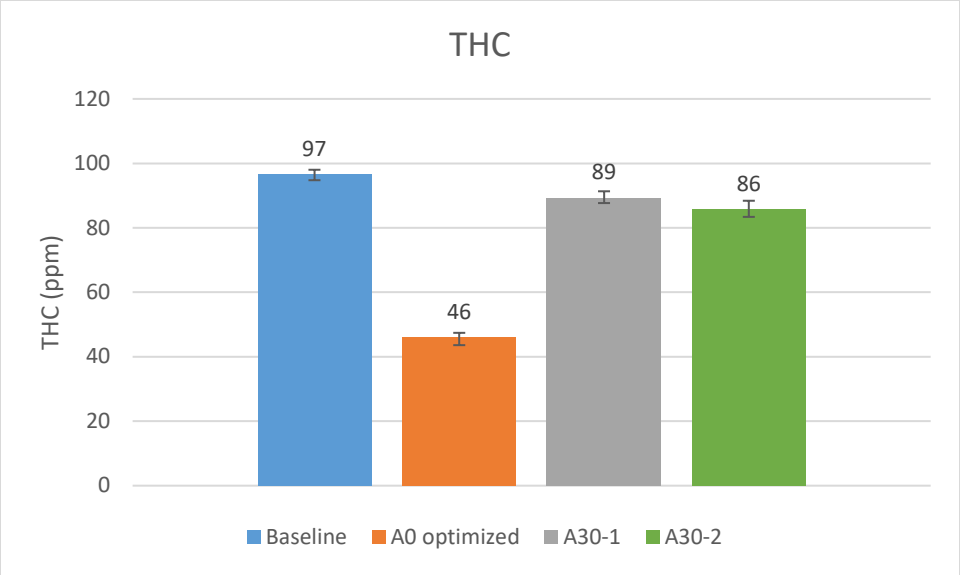

Figure 38: Bar plot for THC emissions for baseline and 3 optimized points. The lowest THC can be observed for A0 optimized test point with maximum reduction of 33% from baseline scenario

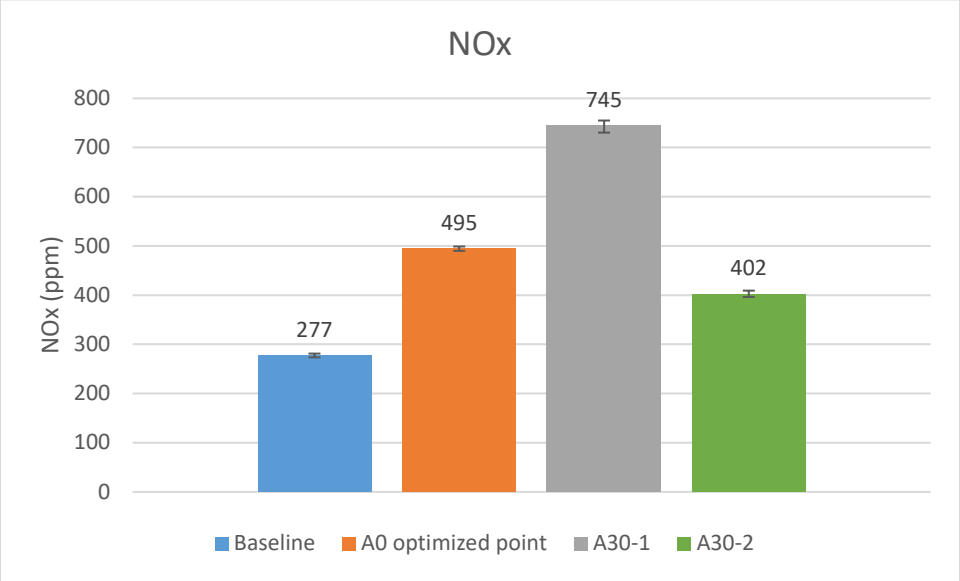

Figure 39: This plot shows the increase that optimization and Biodiesel cause. A NOx of 745 ppm was observed for the highest BTE however, using EGR, more than 50% reduction was achieved.

In the 1.9L engine, a few test points of 30% *n*-hexadecane blend with Marathon diesel were studied to compare the thermodynamics and emissions properties while maintaining NOx parity with the baseline diesel. A reduction in BTE was noticed as compared to the highest efficiency obtained at previously optimized testing point. However, an increase of about 2% point in BTE versus the baseline was noticed even when running at the similar torque and NOx emissions.

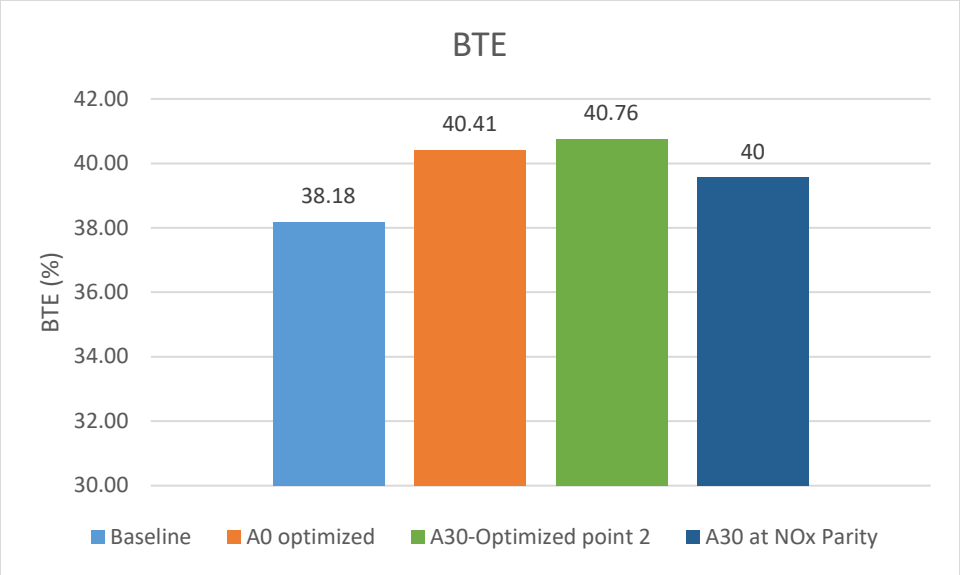

Figure 40: BTE improvement is shown for the baseline, baseline optimized, A30 blend optimized, and A30 blend optimized for NOx parity.

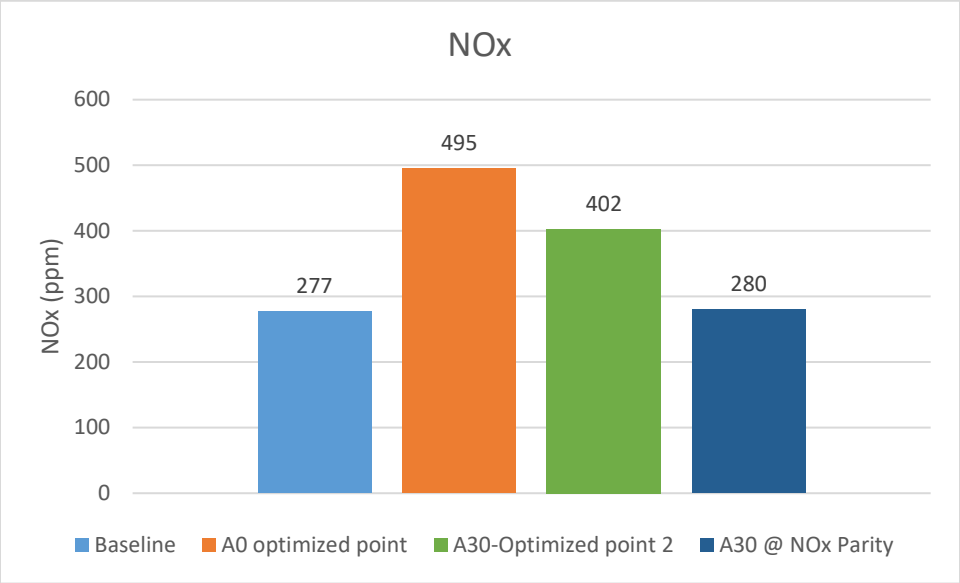

Figure 41: NOx emissions for the baseline, baseline optimized, A30 blend optimized, and A30 blend optimized for NOx parity.

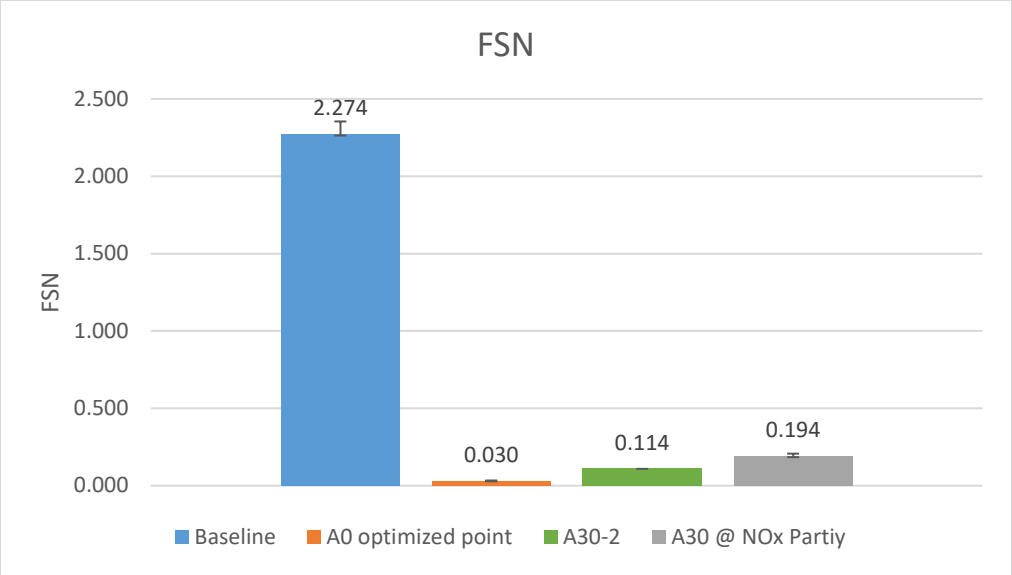

Figure 42: FSN slightly increased in an effort to reduce the NOx emissions to the baseline level.

In the 1.9L engine, a few test points of Marathon baseline diesel and 30% n-hexadecane blend with Marathon diesel were repeated to compare the thermodynamics and emissions properties while maintaining NOx parity with the baseline diesel with an additional instrument to measure emission particles; the Engine Exhaust Particle Sizer also known as EEPS. EEPS, by TSI, was used to study the particle number concentrations in the exhaust. A reduction in BTE was noticed compared to the highest efficiency obtained at the previously optimized testing point for the baseline diesel. However, an increase of about 2% point in BTE versus the baseline was noticed even when running at similar torque and NOx emissions with 30% blended *n*-hexadecane, as shown in Figures 43-46 below.

EEPS also showed an overall reduced concentration of the emission particles for these optimized tests. Similar improvement can be observed in the FSN and NOx emissions for both optimized test points in the figures below. A0_base represents pure marathon baseline diesel at the engine baseline operating conditions and pedal simulations to achieve the desired torque. A30_base is 30% *n*-hexadecane at similar operating conditions, i.e., pedal simulation to achieve the desired torque. A0_opt and A30_opt are the optimized test points for the baseline diesel and the 30% blend with *n*-hexadecane, respectively.

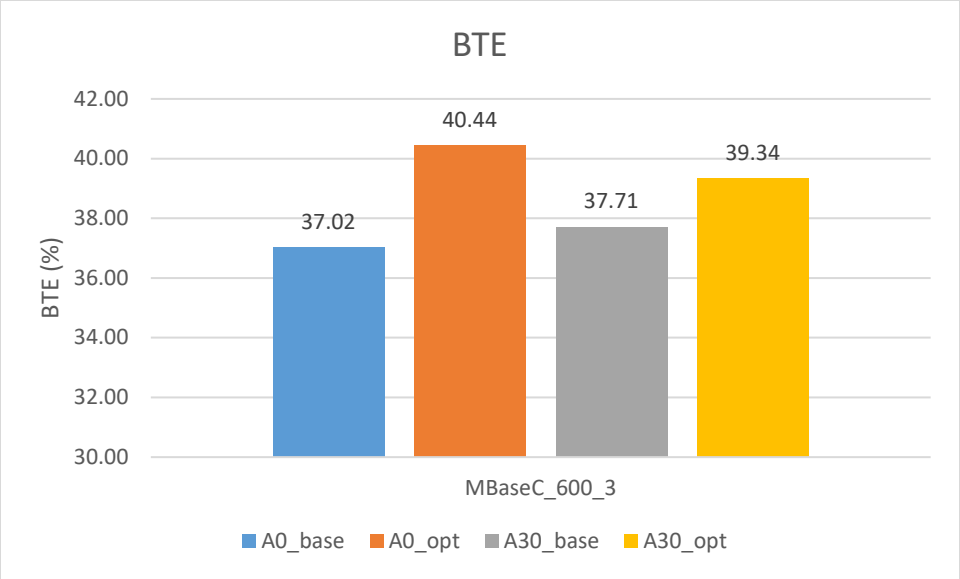

Figure 43: BTE improvement is shown for the baseline diesel at baseline operating conditions, baseline optimized, A30 blend baseline, and A30 blend optimized

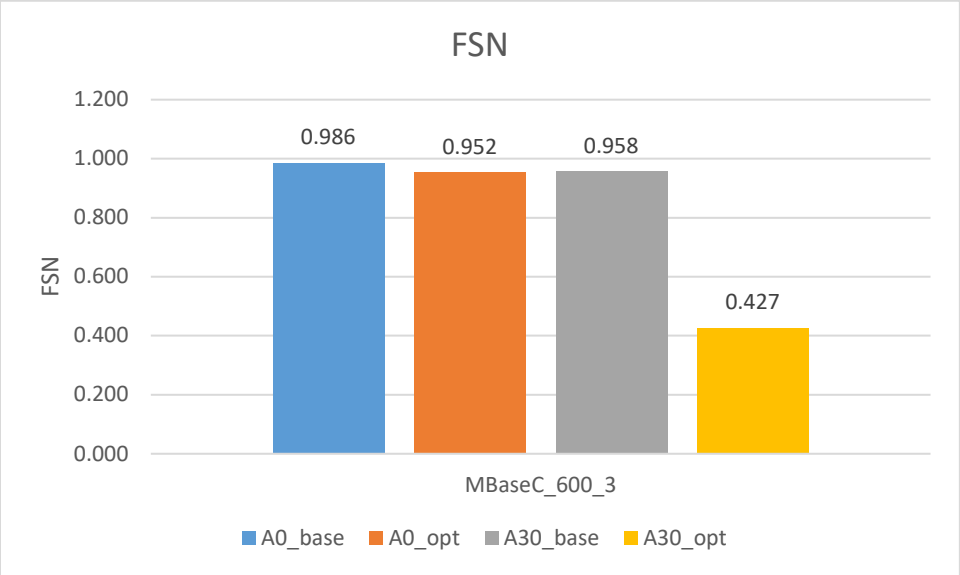

Figure 44: FSN for the baseline diesel at baseline operating conditions, baseline optimized, A30 blend baseline, and A30 blend optimized

Figure 45: NOx emissions reduction is shown for the optimized points for the baseline diesel and A30 blend.

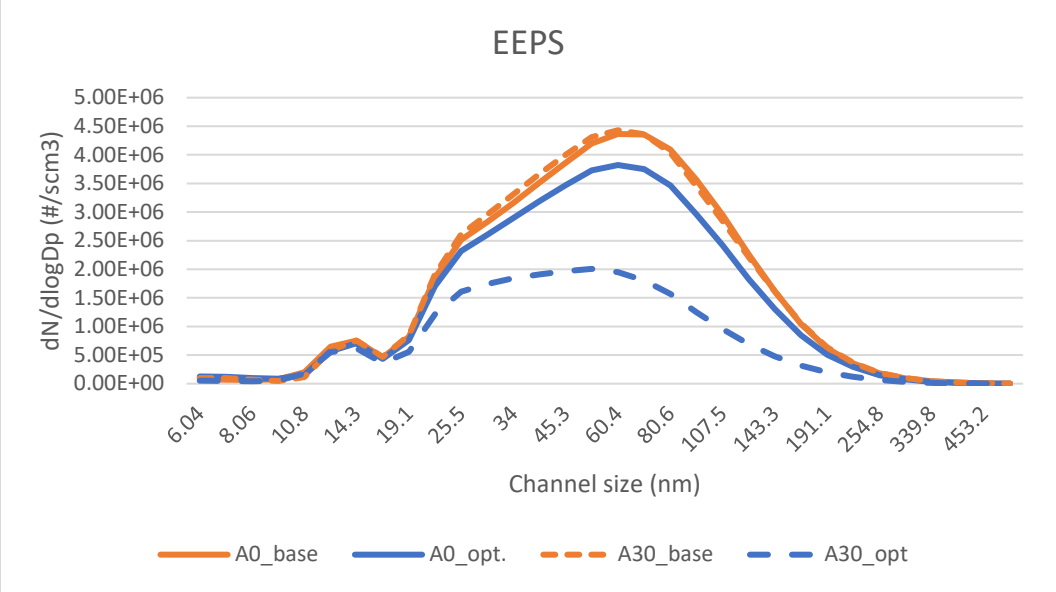

Figure 46: Exhaust particles concentration showed an overall reduction correlated with the optimization for the baseline diesel as well as for the A30 blend.

Heavy-Duty SCRE Studies

After conclusion of the work with the GM1.9L engine, we planned experiments on the modified 11L Volvo heavy-duty engine, which was developed under the Volvo Supertruck 1 and 2 programs. We planned to test 3 different fuels: Marathon diesel as a baseline; “A30” which is 30% *n*-hexadecane

blended with Marathon Diesel; and 100% Renewable Diesel. Like the work done in the light-duty engine, we compared fuel behavior in the heavy-duty engine and achieved optimization for efficiency and emissions. As with the light-duty engine studies, we used a HORIBA MEXA-One emission bench to measure exhaust emissions and but for the heavy-duty engine particle emissions we used a TSI Scanning Mobility Particle Sizer (SMPS) to capture the size distribution of soot particles. Attached are the pictures of the heavy-duty Volvo engine which is equipped with the electrohydraulic Lotus Active Valve Train (AVT) system for full control over the intake and exhaust valve timing, lift, and velocity.

Figure 47: Images of the original Volvo MD11 cylinder head (left) and the modified cylinder head (right) that incorporates the Lotus AVT hydraulic valve actuation system.

The initial set of experiments using Marathon diesel on the Volvo engine were at two operating points A50 and A75 at 1160 RPM speed. A50 corresponds to 11.9 bar net IMEP and A75 to 17.6 bar. Since point A75 operates closer to the on-road cruising conditions, this test condition was selected to further optimize by exploring various strategies such as main Injection timing, pilot injection timing, boost pressure, and EGR. The controlling parameter for the optimization is to get the IMEP of 17.6 bar and achieve the highest efficiency possible with the best emissions reduction.

We successfully conducted experiments on the Volvo MD11 engine using three different fuel types: marathon baseline diesel, a 30% blend of *n*-hexadecane with diesel, and 100% renewable diesel. To optimize the engine performance, we employed our methodology, which utilizes data-based AI modeling and the space filling method offered by ASCMO. Through this approach, we conducted approximately 100 test points, for each fuel, systematically varying injection strategies, intake boost pressure, and EGR, while operating at a medium speed medium load of 1160 rpm and 11.6 net IMEP. It is important to note that this "baseline" operating point had already been optimized by Volvo, serving as our starting point.

Our methodology outperformed traditional sweep testing methods by providing an efficient and accurate means of optimizing engine performance. The results of our experiments showcased the potential of this approach. When compared to the baseline optimized point for the diesel fuel, we observed up to 55% reductions in NOx emissions and up to a 2% reduction in fuel consumption. The utilization of a 30% blend of *n*-hexadecane with diesel further enhanced our findings, resulting in a notable 6% reduction in fuel consumption. Moreover, when utilizing 100% renewable diesel, we observed an impressive 8% reduction in fuel consumption, again when compared to the baseline point operating on marathon diesel.

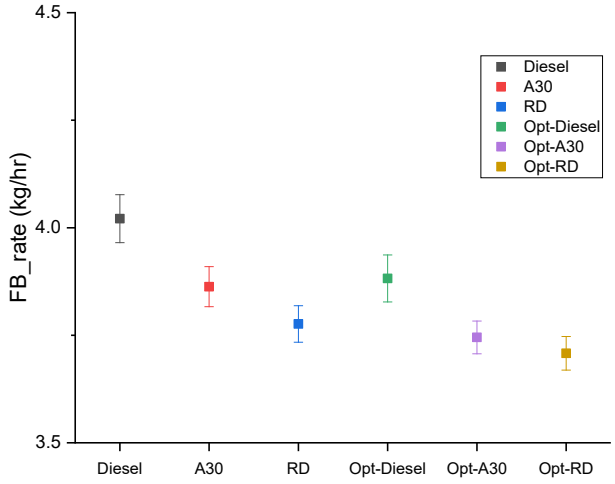

Figure 48: We achieved up to 8% reduction in fuel consumption through utilization of high intake boost pressure, earlier injection, and high Cetane fuel (or fuel blend).

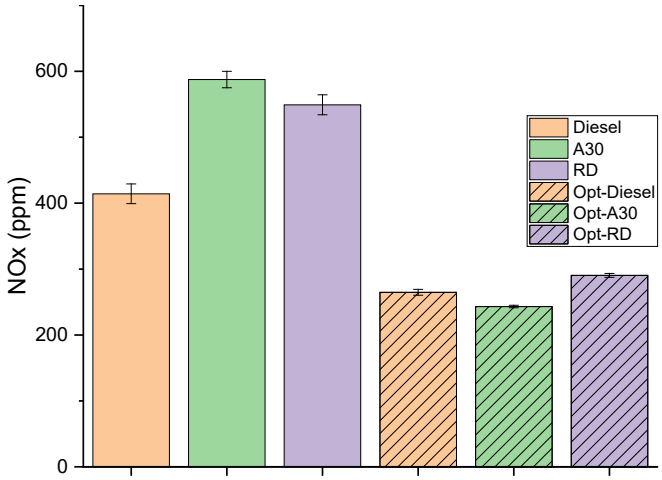

Figure 49: The plot shows an increased NOx emissions for alternate fuels at baseline; however, the optimized points show up to 50% Reduction in NOx Emissions with n-Hexadecane Blend and 100% Renewable Diesel.

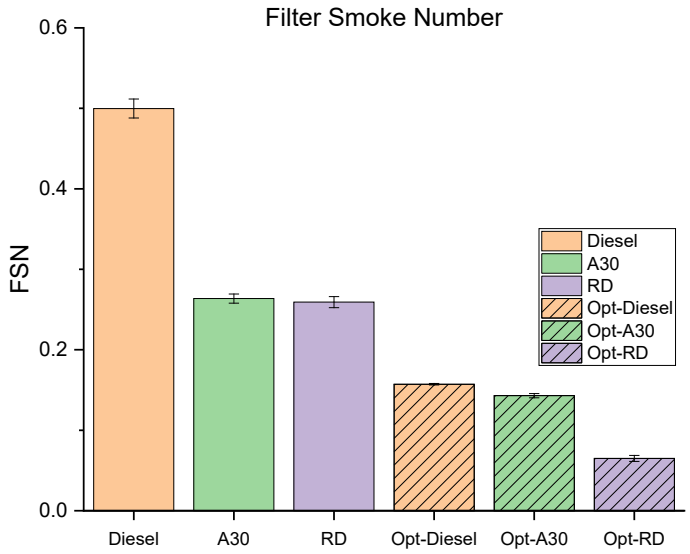

Figure 50: Alternate fuels showed significant reduction in PM at the baseline operating point; however, with further optimization we observed up to 87% improvement for renewable diesel when compared with baseline operating point at Marathon Diesel.

These findings highlight the significant impact that our methodology can have on optimizing engine performance and reducing emissions utilizing alternate fuels such as those derived from algae. By leveraging data-based AI modeling and exploring the potential of low life cycle greenhouse emissions biofuels, such as algae-derived bioblendstocks (represented here as *n*-hexadecane) and renewable diesel, we can make substantial strides in achieving more sustainable and efficient heavy-duty engines. These results serve as a strong foundation for further research and development in the field of engine optimization and alternative fuel utilization, supporting the ongoing efforts to mitigate the environmental impact of transportation systems.

3. ACKNOWLEDGEMENTS

This material is based upon work supported by the U.S. Department of Energy's Office of Energy Efficiency and Renewable Energy (EERE) under the Fiscal Year 2018 Advanced Vehicle Technologies Research Funding Opportunity Announcement (FOA) Number: DE-FOA-0001919, Area of Interest 5b: Bioblendstocks to Optimize Mixing Controlled Compression Ignition (MCCI) Engines, under Award Number DE-EE0008482.

The co-PIs and students who have been involved in this project, wish to thank the U.S. Department of Energy and DOE Bioenergy Technology Office (BETO) for supporting this work. We are grateful for the guidance provided by project and contract managers from DOE, including Alicia Lindauer, Philip Lee, Trevor Smith and Robert Natelson. We are also grateful to Robert McCormick of the National Renewable Energy Laboratory, who has served as the DOE national lab liaison throughout the project, and to Gina Fioroni and Jon Luecke for supporting the bioblendstock property analyses. We are grateful to Dr. Charles McEnally and Zhanhong (Aurora) Xiang of Yale University for their efforts to measure the sooting index teendency of our bioblendstock samples.

We are also grateful to Marathon Petroleum Corporation who have co-funded work and provided essential technical guidance during this project. In particular, we are indebted to Steve McConnell for his unwavering support.

We are also grateful to Shailesh Lopes of General Motors and the Top Tier Fuel program, which donated surplus renewable diesel fuel from a Top Tier supported research program at the University of Michigan that has been used in this study.

4. PROJECT TEAM

Principal Investigator:	André L. Boehman, Ph.D., P.E. Professor of Mechanical Engineering University of Michigan
Co-Principal Investigators:	Bradley Cardinale, Ph.D. Head, Department of Ecosystem Science and Management College of Agricultural Sciences Penn State University
	Daniel C. Haworth, Ph.D. Professor of Mechanical Engineering, Emeritus Penn State University
	Philip Savage Walter L. Robb Family Chair Department Head, Chemical Engineering Penn State University
	Levi Thompson, Ph.D. Elizabeth Inez Kelley Professor of Chemical Engineering Dean, College of Engineering University of Delaware
Research Scientists / Fellows:	Saemin Choi, Ph.D. Research Scientist University of Michigan
	Taehoon Han, Ph.D. Research Fellow University of Michigan
Doctoral Students:	Muhammad Abdullah Graduate Student Research Assistant University of Michigan
	Jun Han, Ph.D. Graduate Research Assistant Penn State University
	Pete Guirguis Graduate Research Assistant Penn State University
Masters Students:	Elana Miyasato Graduate Student Research Assistant University of Michigan

Cansu Dogonay
Graduate Student Research Assistant
University of Michigan

Alex Carley
Graduate Research Assistant
Penn State University

Tim Shokri
Graduate Research Assistant
Penn State University

Spencer Widin
Graduate Student Research Assistant
University of Michigan

Undergraduate Students

Terrence Brannigan
University of Michigan

Ravi Bakshi
University of Michigan

University Research Opportunity Grant Undergraduate Students

Name	School	Department
Brandon Phee	University of Michigan	Mechanical Engineering
Max Mancini	University of Michigan	Mechanical Engineering
Hana Chrenka	University of Michigan	Literature Science and the Arts (LSA)
Joon Kyo Kim	University of Michigan	Aerospace Engineering
Makenzie Womack	University of Michigan	Aerospace Engineering
Daisha Griffin	University of Michigan	Biology
Jalen Hurley	Mott Community College	Associate in Science
Kaitlin Nguyen	Henry Ford College	Business Administration

5.

6. REFERENCES CITED

[1] Widin, S.L., Billings, K.M., McGowen, J., Cardinale, B.J. Biodiversity and disease risk in an algal biofuel system: An experimental test in outdoor ponds using a before-after-control-impact (BACI) design. PLoS ONE 17(4): e0267674 (2022). https://doi.org/10.1371/journal.pone.0267674

[2] Miyasato E. M., Cardinale, B. J. Impacts of Fungal Disease on Algal Biofuel Systems: Using Life Cycle Assessment to Compare Control Strategies, *Environmental Science & Technology 57*(6), 2602-2610 (2023). DOI: 10.1021/acs.est.2c07031

[3] Carruthers, D.N., Goodwin, C.M., Hietala, D.C., Cardinale, B.J., Lin, X. N., Savage, P.E., Biodiversity improves life cycle sustainability metrics in algal biofuel production, *Environ. Sci. Technol.*, **53**, 9279−9288 (2019).

[4] Sterner, C. Advanced Algal Systems. 2021 BETO Peer Review Meeting, March 8, 2021.

[5] Jones et al. Process Design and Economics for the Conversion of Algal Biomass to Hydrocarbons: Whole Algae Hydrothermal Liquefaction and Upgrading. Report PNNL-23227 (2014).

[6] Cheng, S. Ignition Studies in a Motored Engine for Kinetic Mechanism Development and Validation. Ph.D. Thesis, Mechanical Engineering, University of Michigan (2020).

[7] Han, J. CFD Modeling of Ignition and Soot Formation for Advanced Compression-Ignition Engines. Ph.D. Thesis, Mechanical Engineering, Penn State University (2022).

[8] Lilik, G.K. and A.L. Boehman. Effects of Fuel Composition on Critical Equivalence Ratio for Autoignition. *Energy & Fuels,* **27**, 1601–1612 (2013).

[9] Lilik, G.K. and A.L. Boehman. Effects of Fuel Ignition Quality on Critical Equivalence Ratio for Autoignition. *Energy & Fuels,* **27**, 1586–1600 (2013).

[10] Gao, Z., Curran, S., Daw, C., Wagner, R. Light-duty drive cycle simulations of diesel engine-out exhaust properties for an RCCI-enabled vehicle. In 8th US National Combustion Meeting, University of Utah, May, pp. 19–23 (2013). https://www.osti.gov/biblio/1082102.

Appendix A.

Final Milestone Summary related to overall project deliverables. The table below and the descriptions after the table of the final deliverable milestones is a portion of the Statement of Project Objectives (SOPO) milestone table.

Milestone Summary Table							
Task Number	Task or Subtask	Type	Milestone Number	Milestone Description	Verification Process	Months from Start	Quarter from Start
4.3	Optimized Algal Fuel	Milestone	4.3	Production of samples of optimized upgraded algal fuel completed, including 500 ml of sample to be provided to the DOE National Lab team	Reporting to DOE Program Managers through quarterly written reports and teleconferences documenting that the optimized algal fuel yields improvements in cetane number and sooting propensity when used as a bioblendstock	33* (57)	11 (18)
5.3	MCCI Engine Studies	Milestone	5.3	Demonstration of optimized algal fuel in MCCI combustion to assess the benefits of the co-optimized fuel and combustion process	Reporting to DOE Program Managers through quarterly written reports and teleconferences documenting improvements in MCCI combustion	36* (54)	12 (18)

Subtask 4.3: *Scale-up of upgrading of algal biocrude (M12-M36).* Larger quantities of the algal fuel samples will be produced using the pilot-scale reactor system, to support property measurements, combustion and generation of the optimized algal fuels for MCCI combustion. * Completion date was extended to June 30, 2023 (numbers in parentheses indicate actual months and quarters).

Subtask 5.3.2: Engine combustion, performance and emissions experiments using model algal fuel blends in selected base fuels. A GM 1.9L turbodiesel engine and a Volvo MD11 HD SCRE were used to perform combustion, performance and emissions experiments using the model algal fuel (*n*-hexadecane) blended into the base fuel.

Milestone 4.3 Optimized Upgraded Algal Fuel Sample Completed (M33)

In recent quarters, our major outcome has been to find upgrading conditions that are yielding an upgraded HTL blendstock that is soluble in a model diesel fuel and in biodiesel. In this final quarter, as discussed in Section 4, our focus has been on the optimizing the upgraded HTL biocrude. The HTL conversion of algae to biocrude and the upgrading of the biocrude took place in our scale-up reactors. These upgraded biocrude samples contained a wide boiling range. An in-house developed distillation apparatus was used to separate the jet and diesel range material from the lighter and heavier fractions.

Milestone 5.3 Engine Studies and Simulation

In recent quarters, engine optimization studies were expanded from the initial work in a GM 1.9L turbodiesel engine with an open controller (DRIVVEN) to include a Volvo D11 single-cylinder research engine (SCRE) with fully variable valve timing, which had been developed under the Volvo *Supertruck 2* program. Using an industry standard optimization tool (ASCMO), engine control parameters were surveyed, a model generated operating conditions to map the engine-fuel response surface, those operating conditions were studied, and the optimized settings were validated and explored.